

Restoring capability of friction pendulum seismic isolation systems

D. Cardone · G. Gesualdi · P. Brancato

Received: 10 August 2014 / Accepted: 18 December 2014 / Published online: 8 January 2015
© Springer Science+Business Media Dordrecht 2015

Abstract The restoring (or re-centring) capability is an important feature of any isolation system and a fundamental requirement of current standards and guideline specifications for the design of seismically isolated structures. In this paper, the restoring capability of spherical sliding isolation systems, often referred to as friction pendulum systems (FPSs), is investigated through an extensive parametric study involving thousands of non-linear response history analyses of SDOF systems. The dynamic behavior of the isolation system is described with the visco-plastic model of Constantinou et al. (J Struct Eng 116(2):455–474, 1990), considering the variability of the friction coefficient with sliding velocity and contact pressure. Numerical analyses have been carried out using a set of approximately three hundred natural seismic ground motions recorded during different earthquakes and differing in seismic intensity, frequency content characteristics, magnitude, epicentral distance and soil characteristics. Regression analysis has been performed to derive the dependency of the residual displacement from the parameters governing the dynamic response of FPS. The influence of near-fault earthquakes and the accumulation of residual displacements due to real sequences of seismic ground motions have been also investigated. Finally, the restoring compliance criteria proposed in this study are compared to the lateral restoring force requirements of current seismic codes. Based on the results of this study, useful recommendations for a (more) rational design of FPSs are outlined.

Keywords Seismic isolation · Restoring capability · Residual displacements · Friction pendulum system · Friction coefficient

1 Introduction

The restoring capability is identified by current seismic codes as a fundamental requirement of seismic isolation systems to prevent significant residual deformations after an earthquake,

D. Cardone (✉) · G. Gesualdi · P. Brancato
University of Basilicata, Potenza, Italy
e-mail: donatello.cardone@unibas.it

which may affect the functionality of the structure and eventually compromise the maximum displacement capacity of the isolator (Skinner et al. 1993).

The great importance of residual displacements in the design of structures with seismic isolation is clearly stated in the ASCE 7 standards (revision for 2016):

- (i) The restoring force requirement is intended to limit residual displacements in the isolation system resulting from any earthquake event so that the isolated structure will adequately withstand aftershocks and future earthquakes;
- (ii) Permanent offset may affect the serviceability of the structure and possibly jeopardize the functionality of elements crossing the isolation plane (such as fire protection and weather proofing elements, egress/entrance details, elevators, joints of primary piping systems etc.). Since it may not be possible to re-center some isolation systems, isolated structures with such characteristics should be detailed to accommodate these permanent offsets.

The final goal of the re-centring capability of seismic isolators is then twofold: (i) limiting the residual displacement at the end of a single seismic event, (ii) preventing the accumulation of residual displacements after a sequence of seismic ground motions. Insufficient restoring capability may be a critical concern especially for seismically isolated structures located in close proximity to faults where seismic ground motions characterized by pulse-like excitations, highly asymmetric accelerograms and large long-period velocities can be expected (Baker 2007). Near-fault earthquakes, indeed, can give rise to significant residual displacements for isolation systems with inadequate restoring capability (Ismail et al. 2014; Katsaras et al. 2008). Moreover, nonlinear isolation systems designed for high seismic intensities may accumulate significant residual displacements after low-to-moderate seismic intensities earthquakes, during which the isolation system exhibit a higher nonlinear behavior (Shin et al. 2014).

The aforesaid considerations are particularly critical for flat sliding bearings, which do not have any restoring capacity and whose behavior may be also affected by installation defects and imprecisions (Kelly 2001). Structures on flat sliding bearings would likely end up in a different position after an earthquake and accumulate considerable residual displacements due to aftershocks. The development of the friction pendulum system (FPS) (Al-Hussaini et al. 1994; Mokha et al. 1991, 1993), which basically consists in an articulated slider—covered with a low-friction high-bearing material (typically PTFE)—that slides upon a concave spherical sliding surface, has tried to overcome the main limitation of sliding bearings for their use in seismic isolation applications. The restoring mechanism in FPS is strictly related to the gravity force of the mass of the superstructure, which is lifted vertically as the isolation system move laterally (Naeim and Kelly 1999).

In the past, the restoring capability of nonlinear isolation systems has not received sufficient attention by researches and structural engineers. Most of the previous studies on the restoring capability of nonlinear isolation systems, indeed, are mainly focused on the residual displacements of generic low-ductility non linear SDOF systems. For instance, Riddell and Newmark (1979) showed that the magnitude of the residual displacement may be strongly affected by the hysteresis loop shape of the nonlinear system. Mahin and Bertero (1981) found that, for some Elastic-perfectly plastic systems, the residual displacement averaged more than 40% of the peak displacements with significant scatter. Kawashima et al. (1998) proposed a method for estimating the likely residual displacements of SDOF systems as a function of the slope of post-yielding branch. MacRae and Kawashima (1997) found that the residual displacements of bilinear SDOF systems almost totally depends on the stiffness ratio of the bilinear curve.

The lack of attention towards the restoring capability of seismic isolation systems can, perhaps, be explained by the fact that the first seismic isolators to be used were laminated rubber bearings, which are endowed with an adequate self-centering capability related to the elastic restoring force developed in the rubber layers when they undergo shear deformation (Tsopelas et al. 1994). With the introduction in the market of other types of isolator devices, characterized by higher energy dissipation capacity but lower self-centering capability (i.e., lead rubber bearings, sliding isolators with steel hysteretic elements, etc.), the problem of residual displacements come under the spotlight (Braun and Medeot 2000). It is worth reminding that energy dissipation and self-centering capability are two antithetic functions: the restoring capability of the isolation system is decreased by forces that can act away from the origin, such as hysteretic forces (hysteretic dampers, yielding force in lead rubber bearings) and friction forces in sliding bearings. The balance of these counteracting components defines the restoring capability of the isolation system. Medeot (2004) proposed the evaluation of the restoring capability of bilinear hysteretic isolation systems based on the energy criterion $E_S \geq 0.25 E_H$, where E_S is the stored elastic energy and E_H is the hysteretic dissipated energy at the maximum displacement. Dicleli and Buddaram (2006) and Berton et al. (2006) presented the results of parametric studies on bilinear hysteretic isolation systems that show the importance of the characteristic strength of the isolation system for its restoring capability. Katsaras et al. (2008) presented the results of a parametric study on bilinear hysteretic isolation systems, showing that the main parameter that affects the restoring capability of bilinear isolation systems is the ratio between the absolute value of the peak displacement (d_{\max}) and the maximum static residual displacement (d_{rm}), which depends on the shape of the hysteretic cycles of the isolation system. The studies by Katsaras et al. (2008), moreover, clearly proved that the restoring capability of isolation systems depends not only on the system properties but also on the earthquake characteristics. From the statistical analysis of more than one hundred seismic records, the authors conclude that bilinear isolation systems with $d_{\max}/d_{rm} > 0.5$ exhibit negligible residual displacements at the end of the earthquake. Based on the outcomes of shaking table tests, Tsopelas and Constantinou (1994) concluded that isolation systems consisting of sliding bearings, rubber devices and fluid dampers exhibit sufficient restoring capability when the ratio of characteristic strength (at high velocity) to peak restoring force is less or equal to 3. This requirement is equivalent to $d_{\max}/d_{rm} > 0.33$, that is in line with the numerical results by Katsaras et al. (2008).

As pointed out by Cardone (2012), the ground motion characteristics strongly influence also the restoring capability of flag-shaped hysteretic cyclic behaviors, which turns out to be better for high-intensity seismic ground motions, which determine larger lateral displacements, than for low-to-moderate seismic ground motions, that determine smaller lateral displacements. From the statistical analysis of the results of an extensive parametric study of SDOF systems subjected to natural seismic ground motions, Cardone (2012) proved that flag-shaped isolation systems experience negligible residual displacements when $d_{\max}/d_{rm} > 3$.

From the examination of the state-of-the-art is clear that the restoring capability of FPS has not been yet examined in detail, although it can significantly affect the design of such isolation systems, especially when the main scope of the design is to limit the force transmitted to the structure (e.g. like in the seismic retrofitting of existing structures). FPSs are characterized by high vertical load bearing capacity and good energy dissipation capacity, related to the friction resistance between sliding surfaces, with a friction coefficient (μ) between 0.02 and 0.12, depending on sliding velocity, contact pressure, air temperature and state of lubrication (Dolce et al. 2005; Quaglini et al. 2012). Actually, the restoring capability of FPSs is conditioned by the acceptability of the vertical displacement corresponding to the maximum earthquake-induced lateral displacement: both are a function of the radius of curvature (R) of the concave

sliding surface(s). Large radii of curvature are needed to limit vertical displacements while small radii of curvature are required to limit residual horizontal displacements.

In this paper, the restoring capability of FPS is investigated through a comprehensive parametric study using a large set of natural seismic ground motions, including both near-fault and far-fault records. The accrual of residual displacements due to real sequences of seismic ground motions is also investigated. The attention is purposely focused on commercial devices, in the attempt to derive useful recommendations to be used in the practical design of FPSs. Finally, the restoring compliance criteria proposed in this study are compared to the lateral restoring force requirements of current seismic codes for isolation systems.

2 Overview of current seismic code specifications

Current seismic codes for the design of structures with seismic isolation require that the isolation system has an adequate restoring capability, in order to limit the residual displacements that may occur at the end of an earthquake (or may accrue after a sequence of seismic ground motions) below values compatible with the functionality of the structure and the correct behavior of the isolation system. It is worth noting that, by requiring high restoring force, cumulative permanent displacements are avoided and the prediction of displacement demand is accomplished with less uncertainty (Constantinou et al. 2007). By contrast, seismic isolation systems with low restoring force ensure that the force transmitted to the structure is predicted with higher accuracy. However, this is accomplished at the expense of uncertainty in the resulting maximum displacement and the possibility of large residual displacements (Constantinou et al. 2007).

The 2001 California Building Code (CBSC 2001), requires a minimum post-elastic (or post-sliding) stiffness (K_p) such that the force at the design displacement (d_d) minus the force at half the design displacement ($d_d/2$) is greater than $0.025W$. Based on the typical (schematic) cyclic behavior of currently used nonlinear isolation systems (e.g. see Fig. 1), this requirement can be expressed as:

$$K_p d_d \geq 0.05W \quad (1)$$

The 2000 AASHTO Guide Specifications for Seismic Isolation Design (AASHTO 2000), have a more relaxed specification for the minimum restoring force but with constraint on the period:

$$K_p d_d \geq 0.025W \quad (2)$$

$$T_{is} \leq 6 \text{ sec} \quad (3)$$

where T_{is} is the fundamental period corresponding to the post-elastic (post-sliding) stiffness K_p of the isolation system (i.e.: $T_{is} = 2\pi\sqrt{M/K_p}$, M being the mass of the superstructure). The AASHTO Guidelines do not permit the use of isolation systems that do not satisfy these requirements.

The International Building Code (IBC 2006), provides restoring capability requirements that are largely based on the AASHTO provisions. The IBC 2006 Code, on the other hand, specifies that the restoring capability requirement may not be fulfilled if the isolation system does not remain stable under full vertical load and horizontal displacements up to 3.0 times the design displacement (e.g. due to accumulation of residual displacement during aftershocks or after a sequence of seismic events).

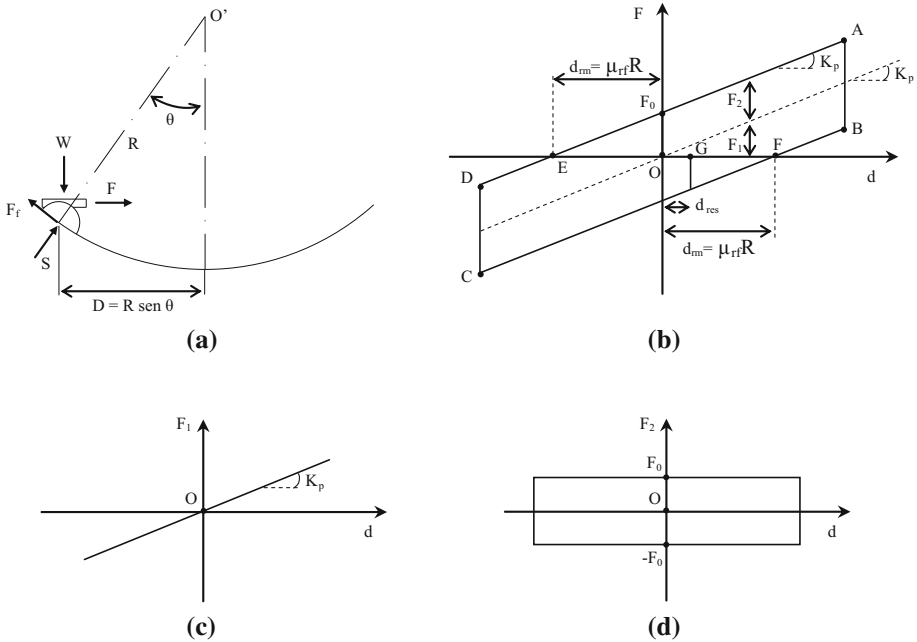


Fig. 1 **a** Working principles of Friction Pendulum System and **b** corresponding idealized bilinear cyclic behavior, resulting from the combination of **c** a linear elastic component and **d** a rigid-perfectly plastic component

The Eurocode 8, EN1998-2 for seismically isolated bridges (CEN 2005) presents a different approach for ensuring sufficient re-centering capability. The Eurocode 8 introduces the concept of maximum residual displacement of the isolating system (d_{rm}), i.e. the residual displacement when the force F_m , required to induce the maximum displacement capacity of the isolation system (d_m), is removed, under quasi-static conditions. The Eurocode 8 requires that the force at the maximum displacement capacity (d_m) minus the force at half the maximum displacement capacity ($d_m/2$) satisfies the following condition:

$$\Delta F_m \geq 0.15W (d_{rm}/d_m) \tag{4}$$

According to EC8-2, expression (4) is valid for:

$$d_{rm} \leq d_m - 0.75d_d \tag{5}$$

It is worth noting that, in all the previous relationships, the restoring force requirement is expressed in absolute terms, i.e. it is not earthquake specific. In principle, this aspect may cause problems in low seismic areas, in which the total restoring force of the isolation system is relatively low. Furthermore, neither of the above criteria is based on solid theoretical fundamentals, rather they make reference to semi-empirical approaches based on experience and experimental evidence, generally valid for a given class of isolation devices (e.g. rubber isolators), characterized by a restoring force that increases with displacement.

3 Theoretical and numerical considerations for FPS

The FPS consists of an articulated slider, typically equipped with PTFE pads, that oscillates around the center of curvature of a concave spherical surface, typically covered by stainless steel shim, whose radius R is equivalent to the pendulum length (Fig. 1a). In Fig. 1a, O' is the centre of curvature of the curved surface, $S = W \cos \theta$ is the resultant of normal pressure acting on the steel-PTFE interfaces, $F_f = \mu W \cos \theta$ is the corresponding friction force during sliding, W is the vertical compression force on the bearing and F is the lateral force at the current lateral displacement d . It's worth noting that equilibrium requires that $S = W \cos \theta - F \sin \theta$, however, $F \sin \theta$ can be neglected with respect to $W \cos \theta$ because the angle θ is very small and F is usually small compared to W . Similarly, it should be noted that the vertical pressure on a bearing supporting weight W consists of three components: (i) pressure due to supported weight, (ii) pressure due to vertical acceleration of the supported weight and (iii) pressure due to overturning moment. In this study, the last two components have been neglected, since they are typically small compared to the first term.

Figure 1b shows the idealized cyclic behavior of FPS, which is defined by two independent parameters, i.e.: the force at zero displacement F_0 (or characteristic strength, equal to the lateral friction resistance μW) and the post-yield stiffness K_p (Fig. 1b). As known (Al-Hussaini et al. 1994), the post-sliding stiffness K_p of single concave FPS is defined as W/R , where R is the effective radius of curvature of the sliding interface, whose commercial values typically range from 2,000 to 4,000 mm (Cardone et al. 2009). Similarly, for double concave FPS with same friction coefficient on the two sliding interfaces, the post-sliding stiffness is defined as $W/(R_1 + R_2)$, R_1 and R_2 being the radii of curvature of the two sliding surfaces. The sliding friction coefficient μ of steel-PTFE interfaces range from 0.02 to 0.12 depending on sliding velocity, contact pressure, air temperature and state of lubrication (Dolce et al. 2005; Quaglioni et al. 2012).

The dynamic behavior of FPS can be captured by combining, in parallel, a linear spring (Fig. 1c) characterized by an elastic force $F_1 = (W/R)d$, modeling the geometry-based re-centring mechanism of FPS, and a rigid perfectly-plastic (RPP) system, defined by a characteristic strength $F_2 = \pm \mu W$ (Fig. 1d), modeling the frictional resistance between sliding surfaces. The RPP component is independent from the displacement d and it points away from the origin when the motion is toward the origin, which may yield to imperfect re-centring of the isolation system.

FPS can be in static equilibrium with zero resultant force under a non-zero residual displacement d_{res} (point G in Fig. 1b). This occurs when the force of the elastic component F_1 equilibrates the force of the frictional component F_2 , i.e.: $F_1 + F_2 = 0$ and this may take place under a residual displacement d_{res} bounded by the maximum static residual displacement d_{rm} , i.e. $-d_{rm} < d_{res} < d_{rm}$ (segment EOF in Fig. 1b), where the limit d_{rm} is defined as F_0/K_p . The value of the maximum static residual displacement d_{rm} depends on the dynamic(-slow) friction coefficient and radius of curvature of FPS:

$$d_{rm} = \mu_{slow} R \quad (6)$$

According to the Eq. (6), the restoring capability of FPS does not depend on the weight of the structure and improves as d_{rm} decreases, because the residual displacements are bounded by this value. This leads to increase the post-sliding stiffness $K_p = W/R$ while reducing the friction resistance $F_0 = \mu W$, in order to improve the re-centring capacity of FPS. In other words, low values of the radius of curvature and friction coefficient can ensure optimal re-centring capability for FPS. However, little values of d_{rm} mean that the linear elastic component dominates the FPS behavior. Consequently a poor energy dissipation capacity

is expected. On the other hand, for an elastic-perfectly plastic system ($R = \infty$), the value of d_{rm} tends to diverge, which means that such a system can be in static equilibrium at any displacement.

One of the most important properties of FPS is that the fundamental period of vibration of the isolated structure (T_{is}) is independent from the mass, being equal to:

$$T_{is} = 2\pi \sqrt{\frac{R}{g}} \tag{7}$$

where g is the gravity acceleration.

The effective damping (ξ_{eq}) of FPS can be expressed as:

$$\xi_{eq} = \frac{2}{\pi} \frac{\mu R}{d} = \frac{2}{\pi} \frac{d_{rm}}{d} \tag{8}$$

The effective damping of FPS depends on displacement amplitude and friction coefficient. The latter varies as a function of sliding velocity, contact pressure, air temperature and state of lubrication. A suitable numerical model for friction is then needed to capture the cyclic behavior of FPS with accuracy.

In this study, the friction model proposed by Constantinou et al. (1990), and recommended for seismic isolation analysis by Nagarajaiah et al. (1991), has been adopted. In this model the friction coefficients μ is velocity-dependent through an exponential analytical law:

$$\mu = \mu_{fast} - (\mu_{fast} - \mu_{slow}) \cdot e^{-rv} \tag{9}$$

where μ_{fast} and μ_{slow} are the friction coefficients at low and fast sliding velocities, respectively, v is the sliding velocity and r is a rate parameter, with dimensions of the inverse of velocity, which depends on contact pressure and air temperature (Dolce et al. 2005).

Equation (9) is in line with experimental outcomes by Constantinou et al. (1987), Hwang et al. (1990), Mokha et al. (1990) and Dolce et al. (2005), which show that the friction coefficient increases more than linearly while increasing sliding velocity. As a consequence, the frictional behavior of FPS is expected to (slightly) change with the frequency content of the earthquake. Moreover, the dynamic-fast friction coefficient μ_{fast} of steel–PTFE interfaces has been found to reduce while increasing contact pressure (Mokha et al. 1990; Dolce et al. 2005). In this study, reference to the experimental laws derived by a leading world manufacturer of FPS has been made (FIP 2013), to take into account the variability of μ_{fast} with axial load:

$$\mu_{fast} = 2.5 \left(\frac{N_{sd}}{N_{Ed}} \right)^{-0.834} \tag{10}$$

$$\mu_{fast} = 5.5 \left(\frac{N_{sd}}{N_{Ed}} \right)^{-0.563} \tag{11}$$

where N_{sd} and N_{Ed} are the quasi-permanent vertical load and maximum load capacity of FPS, respectively. Equations (10) and (11) refer to FPSs with low- and medium-type friction characteristics, respectively. The sliding material utilized in the FPSs under consideration is an Ultra-High Molecular Weight Poly-Ethylene (UHMWPE) coupled with stainless steel.

Considering the typical load working conditions of FPSs ($0.4 < N_{sd}/N_{Ed} < 1.0$), values of μ_{fast} ranging approximately from 2.5 to 5.0% for low-type friction FPSs and from 5.5 to 9.0% for medium-type friction FPSs, respectively, are obtained (see Table 2). The dynamic-slow friction coefficient μ_{slow} has been assumed 2.5 times lower than μ_{fast} (see Table 2), based on the results of experimental tests carried out at the laboratories of the

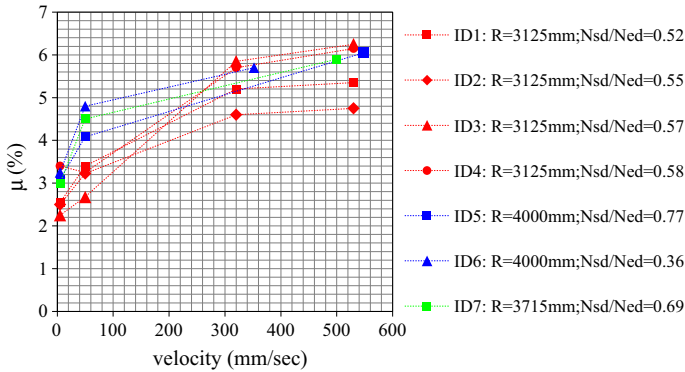


Fig. 2 Experimental variability of the friction coefficient of standard FPSs, as a function of sliding velocity and axial load ratio

University of Basilicata, Potenza (Italy). The tests under consideration include acceptance tests on seven FPSs with characteristics very similar to those considered in this study (low-type friction coefficient, radius of curvature ranging from 3,100 to 4,000 mm, displacement capacity between 250 and 400 mm, axial load ratio ranging from approximately 0.4 to 0.8, air temperature around 20 °C), as well as a number of cyclic tests on flat PTFE-stainless steel interfaces at different levels of bearing pressure (Dolce et al. 2005). In particular, the results of acceptance tests on FPSs (see Fig. 2) point out a ratio between μ_{fast} (at 320–530 mm/s sliding velocity) and μ_{slow} (at about 4 mm/s), on average, around 2.0. The tests on PTFE-stainless steel interfaces, on the other hand, point out ratios between μ_{fast} (at about 320 mm/s) and μ_{slow} (at roughly 2 mm/s) ranging between 2.7 and 3.2 at 20 °C air temperature (Dolce et al. 2005). The choice of assuming in the numerical model $\mu_{fast}/\mu_{slow} = 2.5$ represents a good compromise between the aforesaid experimental outcomes.

Finally, the rate parameter r has been evaluated with the following expression:

$$r = \frac{1}{v_{ref}} \ln \left(\frac{\mu_{fast} - \mu_{slow}}{\mu_{fast} - \mu_{ref}} \right) \tag{12}$$

assuming a reference friction coefficient μ_{ref} equal to 80 % the dynamic-fast friction coefficient μ_{fast} at a reference sliding velocity v_{ref} of 200 mm/s, which is compatible with the maximum sliding velocities expected during an earthquake (Quaglini et al. 2012). A rate parameter r equal to approximately 0.0055 mm/s, has been thus obtained.

It’s worth noting that, strictly speaking, the values of friction coefficient considered in this study are valid for FPSs based on sliding materials similar to those specified above. However, it must be also recognized that the friction coefficient of most currently used FPSs follows similar trends of variation with bearing pressure and velocity and the values of friction coefficient fall in the same ranges under consideration. This implies that the results of this study can be applicable to different types of FPSs with reasonable accuracy.

According to Eqs. (9)–(12), Fig. 3 shows the velocity dependence of the friction coefficient μ assumed in this study for low- (Fig 3a) and medium-type (Fig. 3b) friction FPSs, considering four different values of the axial load ratio N_{sd}/N_{Ed} , ranging from 0.4 to 1.0. It’s worth noting that the reduction of μ , when sliding velocity decreases during the coda phase of the seismic ground motion, is beneficial in terms of re-centring capability of the isolation system, because it corresponds to a reduction of F_0 .

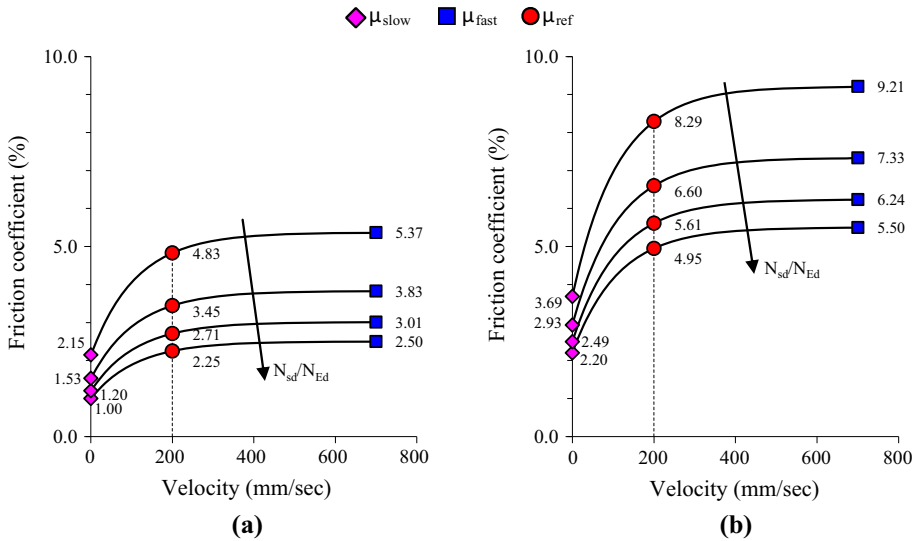


Fig. 3 Variability of the friction coefficient according to the Constantinou’s model, as a function of sliding velocity and contact pressure, for commercial FPSs characterized by **a** low and **b** medium friction characteristics

As argued by [Katsaras et al. \(2008\)](#), the re-centring capability of bilinear isolation systems depends on the entire displacement-time history of their seismic response, which is sensitive to variations in the frequency content of the earthquake. However, the re-centring capability of the system tends to increase for seismic ground motions involving maximum displacements larger than d_{rm} . As a consequence, the ratio d_{max}/d_{rm} appears to be a suitable parameter that can be used to characterize the re-centring capability of nonlinear isolation systems (such as FPS). For FPS, the ratio d_{max}/d_{rm} can alternatively be expressed as $(F_{max} - F_0)/F_0$ (see Fig. 1), i.e. as the ratio between the restoring force at displacements d_{max} to the characteristic strength F_0 . This is a rational comparison because it relates the force increment of the linear elastic component of FPS, whose stiffness K_p (see Fig. 1c) is directly associated to the re-centring capability, with the characteristic strength F_0 of the elastic–perfectly plastic component of FPS (see Fig. 1d), which may trigger imperfect re-centring.

Since the magnitude of the residual displacement significantly depends on the characteristics of the seismic ground motion, a large set of natural seismic ground motions should be used to investigate the re-centring capability of FPSs in a statistical way. The selected seismic records do not need to be compatible with any reference response spectrum, as residual displacements may occur at any seismic intensity. Even better, the selected seismic records should generate a great variety of d_{max} values, in order to really investigate the dependency of residual displacements on d_{max}/d_{rm} .

4 Numerical analyses

The need to evaluate d_{res} , which, as said in the previous section, is bounded by the maximum static residual displacement (i.e.: $-d_{rm} < d_{res} < d_{rm}$), is justified by the great attention devoted by seismic codes and standards (e.g. see ASCE 7, revision for 2016) to the ser-

viceability of structures with seismic isolation, for which residual displacements assumed “a priori” as high as d_{rm} (equal to approximately 136 mm in the worst case under consideration, see Table 2) may result (or just appear) unacceptable. For that reason, if the requirement of limiting residual displacements so that the isolated structure can adequately withstand after-shocks and future earthquakes could be addressed (in first approximation and conservatively) by comparing the lower bound of the residual displacement capacity ($d_m - d_{rm}$) with the maximum displacement d_{max} , it is still essential to evaluate the expected residual displacement d_{res} under low-to-moderate intensity earthquakes or at least to have a criterion to judge whether a given isolation system is prone to the accrual of significant residual displacements under serviceability limit states.

4.1 Selected seismic ground motion and analysis parameters

In this paragraph, the restoring capability of currently used FPSs is investigated in a statistical way, evaluating their residual displacements after a variety of earthquakes. A number of analyses have been also performed to assess the potential of accumulation of residual displacements after a sequence of seismic ground motions. To this end, a set of 280 seismic ground motions, derived from 113 different seismic events, has been selected. The set includes near-fault and far-fault earthquakes, as shown in Table 1. All the seismic records have been obtained from the following databases: (i) ITACA (<http://itaca.mi.ingv.it/>), (ii) ESD (http://www.isesd.hi.is/ESD_Local/frameset.htm), (iii) COSMOS (<http://www.cosmos-eq.org/>) and (iv) PEER (<http://peer.berkeley.edu/nga>). In Fig. 4 the selected seismic ground motions are classified based on (i) Magnitude, (ii) Fault distance, (iii) Peak Ground Acceleration (PGA) and (iv) Soil type.

Table 1 Seismic ground motions considered in the nonlinear response-time history analyses

Seismic event	No. records	Date	Ms	Dist. (Km)	Soil type**	PGA(g)
San Fernando, USA	1(1)*	1971	6.6	2.8	B	1.23
Coyote Lake, USA	1(1)*	1979	5.6	3.1	B	0.43
Imperial Valley, USA	6(5)*	1979	6.9	0.6–23.8	C	0.13–0.46
Mammoth Lakes, USA	2	1980	5.7	–	–	0.35–0.5
Mammoth Lakes, USA	1	1983	5.2	–	–	0.15
Coalinga, USA	1	1983	6.5	–	–	0.16
Morgan Hill, USA	3	1984	6.1	12.8	D	0.16–0.35
N. Palm Springs, USA	3(1)*	1986	6	8–10.1	B	0.22–0.59
Loma Prieta, USA	3(2)*	1989	7.1	11.2–13	A–B–C	0.37–0.51
Petrolia, USA	1	1991	6	–	–	0.50
Cape Mendocino/Petrolia, USA	3	1992	7.1	8.5–18.5	A–B–C	0.55–1.5
Landers, USA	3	1992	7.5	11.6–23.2	B	0.16–0.27
Petrolia, USA	1	1992	6.6	–	–	0.49
Northridge, USA	4(4)*	1994	6.7	6.2–8	A–C	0.42–0.84
Kobe, Japan	2(2)*	1995	6.9	0.3–1.2	D	0.61–0.69
Michoacan, Mexico	2	1997	7.1	17	A	0.36–0.4
Guerrero, Mexico	2(2)*	1997	5	5	A	0.25–0.41
Kocaeli, Turkey	1(1)*	1999	7.8	17	A	0.24
Chi-Chi, Taiwan	2(2)*	1999	7.6	9–14.9	C	0.11–0.28

Table 1 continued

Seismic event	No. records	Date	Ms	Dist. (Km)	Soil type**	PGA(g)
Hector Mine, USA	1	1999	7.1	–	–	0.16
Big Bear City, USA	1	2003	5.4	–	–	0.19
Parkfield, USA	6	2004	6	–	–	0.16–0.68
Sierra El Mayor, USA	1	2010	7.3	–	–	0.16
Kefallinia island, Greece	1	1972	6.37	–	A	0.17
Azores, Portugal	2(2)*	1973	5.31	2	E	0.20–0.27
Ionian, Greece	2	1973	5.78	11	C	0.25–0.52
Gazli, Uzbekistan	2(2)*	1976	7.05	4	D	0.62–0.72
Denizli, Turkey	2(2)*	1976	5.11	3	B	0.26–0.35
Izmir, Turkey	1	1977	5.02	–	B	0.21
Ardal, Iran	1(1)*	1977	5.89	4	A	0.91
Tabas, Iran	2	1978	7.41	14	A	0.34–0.39
Montenegro	10(*4)	1979	6.3–7	3–15	A–B	0.18–0.45
Dursunbey, Turkey	2	1979	4.99	6	B	0.22–0.29
Banja Luka, Bosnia-Herzegovina	5(2)*	1981	5.5	4–7	D	0.22–0.44
Alkion, Greece	2	1981	6.68	10	C	0.23–0.31
Kefallinia, Greece	2	1983	6.1	17	B	0.18–0.23
Panislir, Turkey	2	1983	6.74	17	B	0.13–0.16
Kalamata, Greece	4(4)*	1986	5.77	2	B	0.21–0.3
Tirana, Albania	2	1988	5.59	6	A	0.11–0.41
Chenoua, Algeria	2	1989	5.67	10	C	0.23–0.29
Manjil, Iran	2	1990	7.46	6	–	0.54–0.60
Racha, Georgia	2	1991	5.36	–	C	0.35–0.51
Erzincan, Turkey	2(2)*	1992	6.89	1	B	0.39–0.51
Patras, Greece	2	1993	5.39	–	B	0.15–0.34
Pyrgos, Greece	2	1993	5.08	–	C	0.15–0.43
Firuzabad, Iran	6	1994	5.8	–	A–B	0.25–0.49
Dinar, Turkey	2(2)*	1995	6.04	3	C	0.27–0.32
Kozani, Greece	2	1995	6.51	14	A	0.14–0.21
Kalamata, Greece	1	1997	6.4	–	A	0.12
Sarein, Iran	2	1997	6.1	–	–	0.52–0.56
Adana, Turkey	2(2)*	1998	6.2	4	C	0.22–0.27
Faijal, Portugal	2	1998	6.1	–	C	0.38–0.42
Duzce, Turkey	10(2)*	1999	7.3	1–18	C	0.20–0.8
Izmit, Turkey	9(3)*	1999	5.8–7.8	3–38	A–B–C	0.13–0.61
Karebas, Iran	2	1999	6.3	–	–	0.32–0.36
South Iceland	20(6)*	2000	6.6	3–20	A–B	0.21–0.72
Avej, Iran	2	2002	6.4	22	A	0.43–0.45
Bingol, Turkey	2	2003	6.4	10	A	0.30–0.51
Bam, Iran	2(2)*	2003	6.8	–	B	0.64–0.8
Olfus, Iceland	6	2008	6.2	–	A	0.22–0.66
Friuli, Italy	12(2)*	1976	5–6.4	4–23.4	A–B–C	0.19–0.65
Friuli, Italy	2	1977	5.3	7.1	B	0.18–0.25

Table 1 continued

Seismic event	No. records	Date	Ms	Dist. (Km)	Soil type**	PGA(g)
Patti, Italy	1	1978	6	18.3	C	0.16
Val Nerina, Italy	1	1979	5.8	9.3	B	0.20
Val Nerina, Italy	1	1980	5	10.6	B	0.19
Irpinia, Italy	4	1980	6.9	18.8–42.2	B	0.17–0.32
Basilicata, Italy	1	1981	5.2	12.1	C	0.17
Gubbio, Italy	2	1984	5.6	20.6–26	B–E	0.17–0.21
Val Comino, Italy	2	1984	5.5	8.5–17.4	B	0.16–0.20
East Sicily, Italy	1	1990	5.6	31.2	D	0.25
Parma, Italy	1	1996	5.4	13.3	C	0.20
Umbria Marche, Italy	18(4)*	1997	5.4–6	2.7–24.2	A–B–C–D–E	0.15–0.53
App. Umbro Marchigiano, Italy	4	1998	5–5.1	6.9–10	B–C–E	0.19–0.58
App. Lucano, Italy	2	1998	5.6	6.6–9.8	B	0.16–0.24
L’Aquila, Italy	20(7)*	2009	5–6.3	1.8–18.14	A–B–C	0.16–0.68
Emilia, Italy	29(6)*	2012	5.1–6.1	1.41–21.30	C	0.16–0.51
Calabria, Italy	3(1)*	2012	5.3	1.69–8.35	A–B–C	0.18–0.24
Toscana, Italy	1	2013	5.4	9.47	E	0.23

* Pulse-like records according to (Baker 2007)

** USGS soil classification

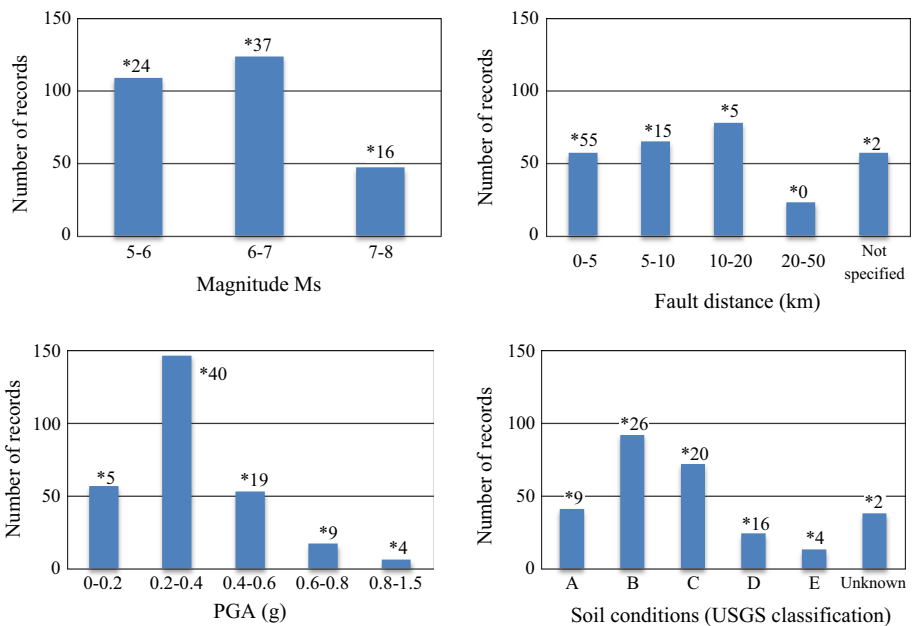


Fig. 4 Classification of the seismic ground motions selected for the analysis. * Number of pulse-like seismic ground motions according to (Baker 2007)

It is worth noting that a number of earthquakes of Table 1 can be classified as “pulse-like” seismic ground motions, according to the criterion proposed by Baker (2007), which uses wavelet analysis to identify velocity pulses in Near-Fault earthquakes. Indeed, the probability of occurrence of pulse-like seismic ground motions is higher (85–95 %) for small source-site distances ($< 4 - 5$ km), while it decreases to zero for source-site distances greater than 30 km (Baker 2007). Pulse-like earthquakes, often resulting from directivity effects, are characterized by a strong pulse in the velocity-time history of the normal-fault component of ground motion.

A key parameter of pulse-like seismic ground motions is the so-called “pulse period” T_p , which is the period corresponding to the dominant peak of the velocity response spectrum. As shown in Baker (2007), the pulse period T_p is linearly correlated to the earthquake magnitude (M_s) and it greatly affects the seismic response of the structure (Anderson and Bertero 1987; Alavi and Krawinkler 2001; Mavroeidis et al. 2004). Earthquakes with pulse-like characteristics have been found to impose extreme demands on structures, to an extent not predicted by typical approaches such as with response spectra (Bertero et al. 1978; Luco and Cornell 2007). Basically, the occurrence of pulse-like seismic ground motions is particularly unfavorable for structures with inadequate restoring capability as it may imply large transient and residual displacements, which basically are not covered by current code provisions. As a consequence, the restoring capability of FPS must be checked against the occurrence of pulse-like seismic ground motions.

In this study, Nonlinear Response History Analyses (NRHA) have been carried on SDOF systems with 100 tons mass, schematizing typical medium-rise residential buildings.

The effects of the vertical component of the seismic ground motion have been neglected. Similarly, the effects of possible auxiliary viscous dampers and the variability of the axial load, due to rocking movements of the building, are not examined in this study.

The numerical model has been implemented in the structural analysis program [SAP2000_Nonlinear \(2014\)](#) using a nonlinear “friction pendulum isolator” link element to model the cyclic behavior of the isolation system. The “friction pendulum isolator” link element of SAP2000 is based on the friction model by (Constantinou et al. 1990), represented by Eq. (9). Friction forces are directly proportional to the compression axial force and the element cannot carry axial tension.

The values of the fundamental mechanical parameters of FPS (i.e., the radius of curvature R and the friction coefficient μ) have been varied during NRHA, to cover the range of values reported in the commercial catalogues of FPSs currently available in Europe. In particular, three commercial values of the radius of curvature R have been considered, equal to 2,100, 3,100 and 3,700 mm, respectively (see Table 2). The values of the dynamic-fast friction coefficient μ_{fast} have been derived from Eqs. (10) and (11), for low- and medium-type friction FPSs, respectively, considering four different values of the axial load ratio N_{sd}/N_{Ed} , equal to 1.0, 0.8, 0.6 and 0.4, respectively. As a result, eight different values of μ_{fast} (and correspondingly of μ_{slow}), ranging from approximately 2.5–9 % (and from 1 to 3.5 %), have been considered in the NRHA (see Table 2). Although the effects of air-temperature variations and maintenance conditions of sliding surfaces (Dolce et al. 2005) have been not directly considered in the analysis, it can be deemed that they are indirectly covered by the large range of axial load ratio (N_{sd}/N_{Ed}), hence friction coefficient, taken into account.

It is worth noting that, according to the indications of the FPS manufacturers, the maximum displacement capacity d_m of FPS change with its radius of curvature R . In this study, reference to the maximum displacement capacities currently available in the commercial catalogues of one leading Italian manufacturer of FPS has been made. The standard FPSs under consideration include double concave curved surface(s) systems with displacement capacity and

radius of curvature of 100–150 mm for $R = 2,500$ mm, 200–250 mm for $R = 3,100$ mm and 300–400 mm for $R = 3,700$ mm, respectively. It should be noted that there are at least three other leading manufacturers in Europe (based in Italy, Germany and Switzerland, respectively) that sell standard FPSs with similar characteristics in terms of friction coefficient, radius of curvature and maximum displacement capacity. As a consequence, the FPS characteristics considered in this study can be considered representative of the current manufacturing standards in Europe.

Table 2 Main characteristics of the commercial FPSs considered in the analysis

FPS type	R (mm)	Max displacement capacity	N_{sd}/N_{ed}	μ_{fast}	μ_{slow}	d_{rm} (mm)
Low-type friction	2,500	100	1.00	0.025	0.010	25.00
Low-type friction	2,500	150	1.00	0.025	0.010	25.00
Low-type friction	3,100	200	1.00	0.025	0.010	31.00
Low-type friction	3,100	250	1.00	0.025	0.010	31.00
Low-type friction	3,700	300	1.00	0.025	0.010	37.00
Low-type friction	3,700	350	1.00	0.025	0.010	37.00
Low-type friction	3,700	400	1.00	0.025	0.010	37.00
Low-type friction	2,500	100	0.80	0.030	0.012	30.11
Low-type friction	2,500	150	0.80	0.030	0.012	30.11
Low-type friction	3,100	200	0.80	0.030	0.012	37.34
Low-type friction	3,100	250	0.80	0.030	0.012	37.34
Low-type friction	3,700	300	0.80	0.030	0.012	44.57
Low-type friction	3,700	350	0.80	0.030	0.012	44.57
Low-type friction	3,700	400	0.80	0.030	0.012	44.57
Low-type friction	2,500	100	0.60	0.038	0.015	38.28
Low-type friction	2,500	150	0.60	0.038	0.015	38.28
Low-type friction	3,100	200	0.60	0.038	0.015	47.47
Low-type friction	3,100	250	0.60	0.038	0.015	47.47
Low-type friction	3,700	300	0.60	0.038	0.015	56.65
Low-type friction	3,700	350	0.60	0.038	0.015	56.65
Low-type friction	3,700	400	0.60	0.038	0.015	56.65
Low-type friction	2,500	100	0.40	0.054	0.021	53.68
Low-type friction	2,500	150	0.40	0.054	0.021	53.68
Low-type friction	3,100	200	0.40	0.054	0.021	66.56
Low-type friction	3,100	250	0.40	0.054	0.021	66.56
Low-type friction	3,700	300	0.40	0.054	0.021	79.45
Low-type friction	3,700	350	0.40	0.054	0.021	79.45
Low-type friction	3,700	400	0.40	0.054	0.021	79.45
Medium-type friction	2,500	100	1.00	0.055	0.022	55.00
Medium-type friction	2,500	150	1.00	0.055	0.022	55.00
Medium-type friction	3,100	200	1.00	0.055	0.022	68.20
Medium-type friction	3,100	250	1.00	0.055	0.022	68.20
Medium-type friction	3,700	300	1.00	0.055	0.022	81.40
Medium-type friction	3,700	350	1.00	0.055	0.022	81.40

Table 2 continued

FPS type	R (mm)	Max displacement capacity	N_{sd}/N_{ed}	μ_{fast}	μ_{slow}	d_{rm} (mm)
Medium-type friction	3,700	400	1.00	0.055	0.022	81.40
Medium-type friction	2,500	100	0.80	0.062	0.025	62.36
Medium-type friction	2,500	150	0.80	0.062	0.025	62.36
Medium-type friction	3,100	200	0.80	0.062	0.025	77.33
Medium-type friction	3,100	250	0.80	0.062	0.025	77.33
Medium-type friction	3,700	300	0.80	0.062	0.025	92.30
Medium-type friction	3,700	350	0.80	0.062	0.025	92.30
Medium-type friction	3,700	400	0.80	0.062	0.025	92.30
Medium-type friction	2,500	100	0.60	0.073	0.029	73.33
Medium-type friction	2,500	150	0.60	0.073	0.029	73.33
Medium-type friction	3,100	200	0.60	0.073	0.029	90.93
Medium-type friction	3,100	250	0.60	0.073	0.029	90.93
Medium-type friction	3,700	300	0.60	0.073	0.029	108.52
Medium-type friction	3,700	350	0.60	0.073	0.029	108.52
Medium-type friction	3,700	400	0.60	0.073	0.029	108.52
Medium-type friction	2,500	100	0.40	0.092	0.037	92.13
Medium-type friction	2,500	150	0.40	0.092	0.037	92.13
Medium-type friction	3,100	200	0.40	0.092	0.037	114.24
Medium-type friction	3,100	250	0.40	0.092	0.037	114.24
Medium-type friction	3,700	300	0.40	0.092	0.037	136.35
Medium-type friction	3,700	350	0.40	0.092	0.037	136.35
Medium-type friction	3,700	400	0.40	0.092	0.037	136.35

The device characteristics, and relevant working conditions, considered in this study are summarized in Table 2. A total of 24 different SDOF systems (3 radii of curvature by 8 friction laws) have been examined and some 6720 NRHA (24 systems by 280 seismic ground motions) have been performed. The maximum transient displacements d_{max} and the residual displacements at the end of the earthquake d_{res} have been registered and then statistically processed, as shown in the next paragraphs.

It is worth noting maximum displacements a little larger (say up to 25 %) than the maximum displacement capacity of the selected FPSs have been accepted, in order to extend the range of analysis, assuming that, in principle, it is possible to manufacture “ad hoc” devices with same radius of curvature and slightly greater displacement capacity. Results out of these ranges have been neglected. This choice reduced the number of analysis cases considered from 6,720 to approximately 5,000.

4.2 Estimation of the residual displacement

Figure 5 shows the changes in the cyclic response of the isolation system registered during a given seismic event (Earthquake: Dinar (Turkey), year: 1995, $M_s = 6.04$, station: Dinar-Meteoroloji Mudurlugu, fault distance: 8 km, $PGA = 0.32 g$), considering different values of

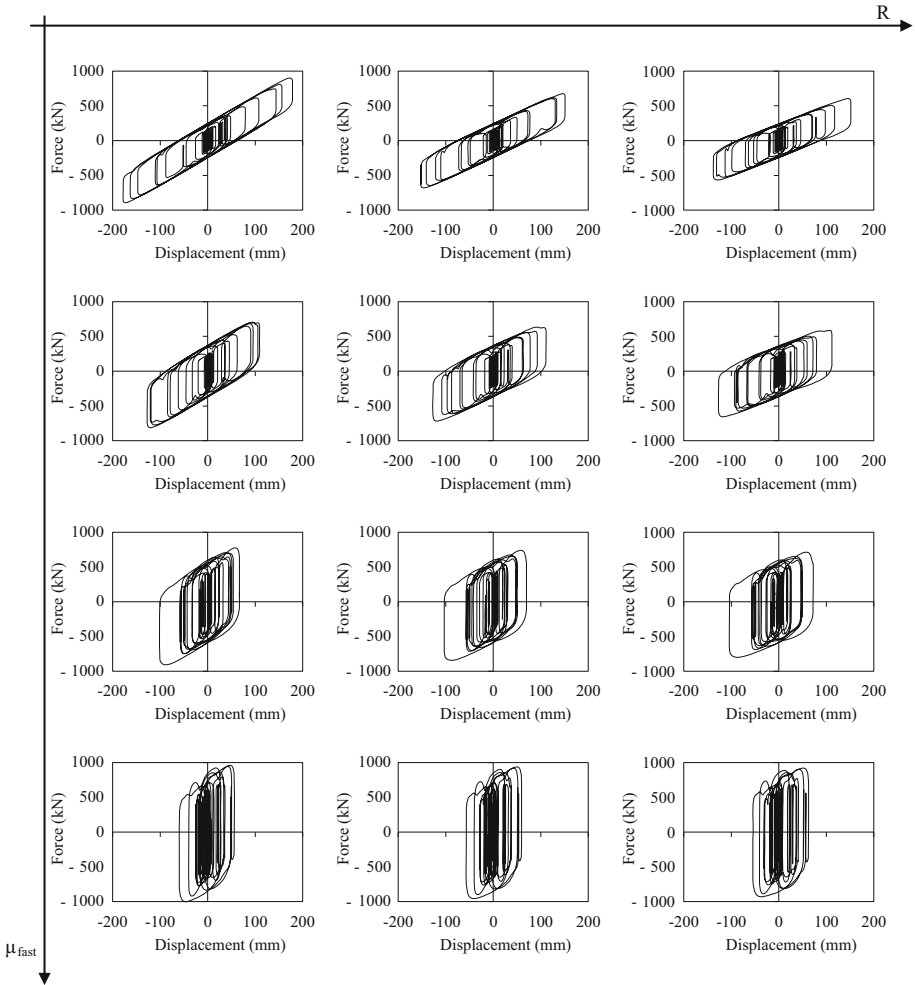


Fig. 5 Changes in the cyclic response of FPS while increasing the radius of curvature ($R=2,500, 3,100, 3,700$ mm) and dynamic-(fast) friction coefficient ($\mu_{fast} = 2.50, 3.83, 6.24, 9.21$ %), for a given seismic ground motion (Dinar-Turkey, year: 1995, $M_s = 6.04$, station: Dinar-Meteoroloji Mudurlugu, fault distance: 8 km, $PGA=0.32$ g)

the friction coefficient ($\mu_{fast} = 2.50, 3.83, 6.24, 9.21$ %) and radius of curvature ($R = 2,500, 3,100, 3,700$ mm).

Figure 6 compares the displacement-time histories of FPSs characterized, alternatively, by different values of friction coefficient (and the same radius of curvature $R = 3,100$ mm, see Fig. 6a) and different values of radius of curvature (and a given friction coefficient $\mu_{fast} = 3.83$ %, see Fig. 6b). As can be seen, if the restoring capability is suitable (Fig. 6b), the residual displacement is little affected by changes of the radius of curvature. On the other hand, if the restoring capability is not adequate (Fig. 6a), the residual displacement (as well as the maximum transient displacement) changes significantly, when the friction coefficient increases from 2.5 to 9.21 %. The residual displacement is negligible when the friction coefficient is 2.5 %, 40 mm when the friction coefficient is 6.24 % and 50 mm when

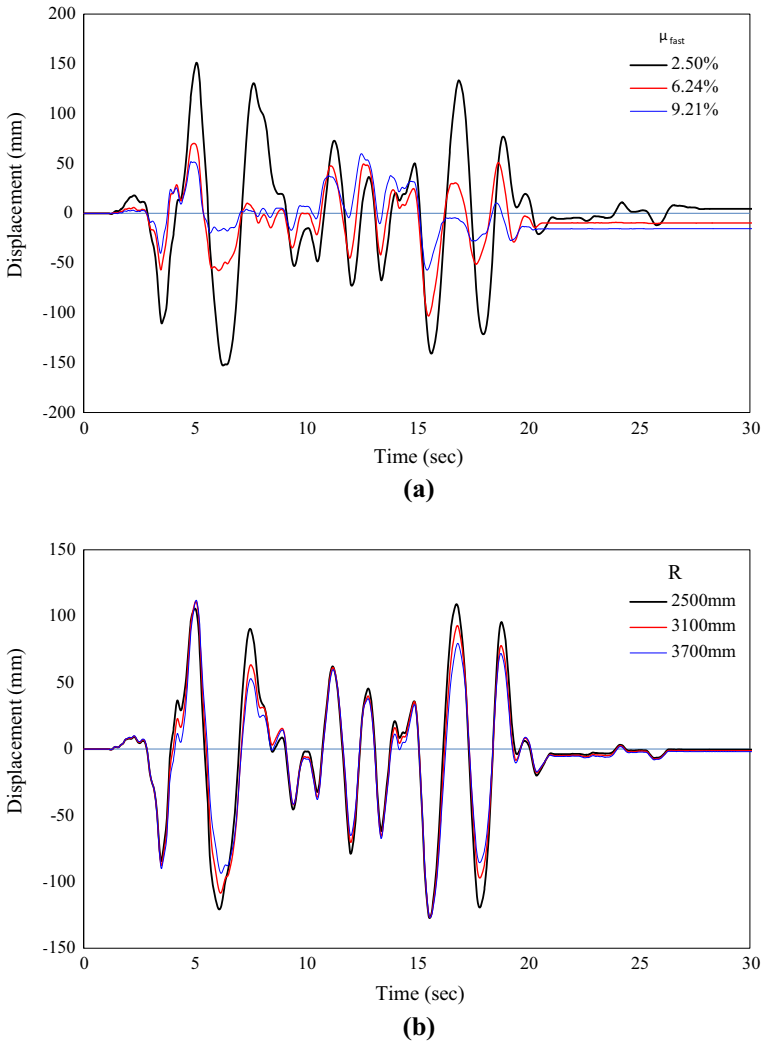


Fig. 6 Comparison between the displacement-time histories of selected FPSs differing in **a** dynamic friction coefficient (for a given radius of curvature, $R=3,100$ mm) and **b** radius of curvature (for a given friction coefficient, $\mu_{fast} = 3.83\%$). Seismic ground motion: Dinar (Turkey), year: 1995, $M_s = 6.04$, station: Dinar-Meteoroloji Mudurlugu, fault distance: 8 km, $PGA = 0.32$ g

the friction coefficient is 9.21 %. In the first case, the system has good re-centering properties and little energy dissipation capacity, while in the other two cases the system has better energy dissipation capacity but worse re-centering capability.

It is important to note that, for a given isolation system, the residual displacement seems to be, to some extent, correlated with the maximum (static) residual displacement: the higher the maximum (static) residual displacement the higher the actual residual displacement, in line with the results reported by [Katsaras et al. \(2008\)](#) and [Cardone \(2012\)](#) for bilinear and flag-shaped isolation system, respectively.

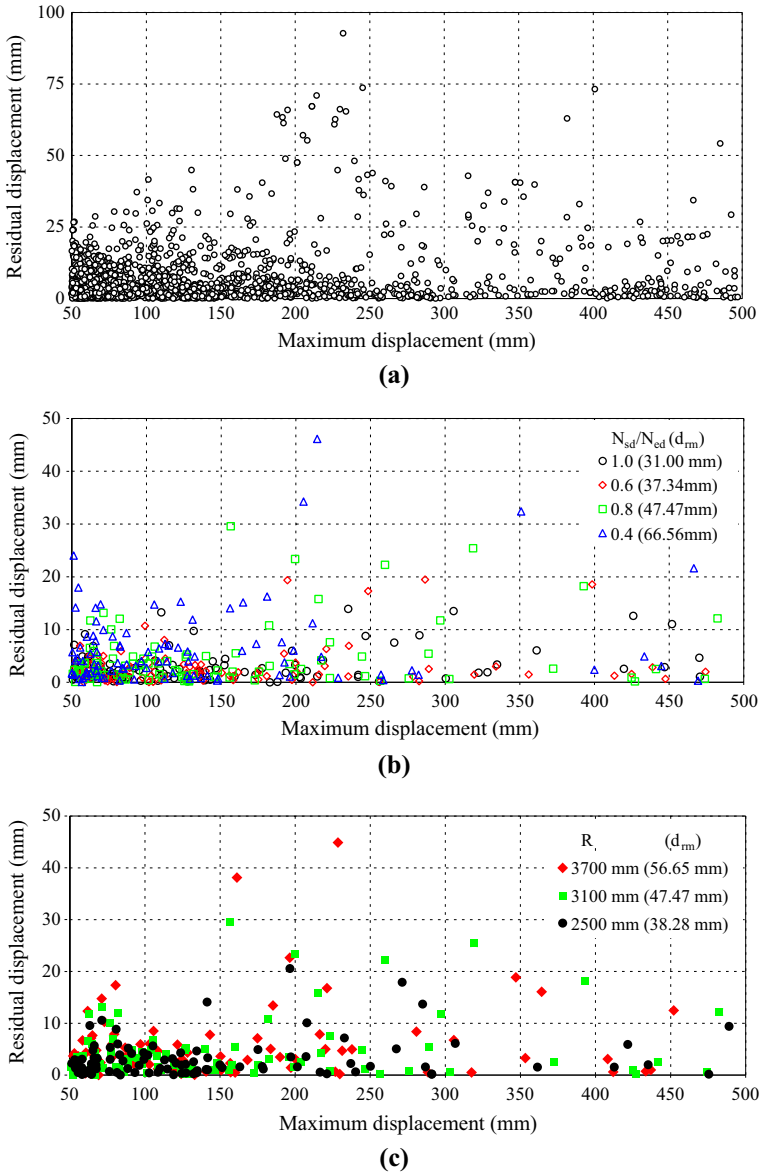


Fig. 7 **a** Residual displacements (d_{res}) vs. maximum displacements (d_{max}) obtained from nonlinear response history analysis; **b** results relevant to low-type FPS with $R = 3, 10, 2500$ mm and **c** low-type FPS with $N_{sd}/N_{ed} = 0.6$

In Fig. 7 the residual displacements obtained from NRHA are reported as a function of the corresponding maximum seismic displacements. As said before, the attention is focused on the range of maximum displacements 50–500 mm, where the maximum displacements of buildings with seismic isolation, that are not located in close proximity to active faults, typically fall (Cardone et al. 2010), considering both serviceability and collapse prevention limit states. As can be seen in Fig. 7a, the residual displacements recorded at the end of

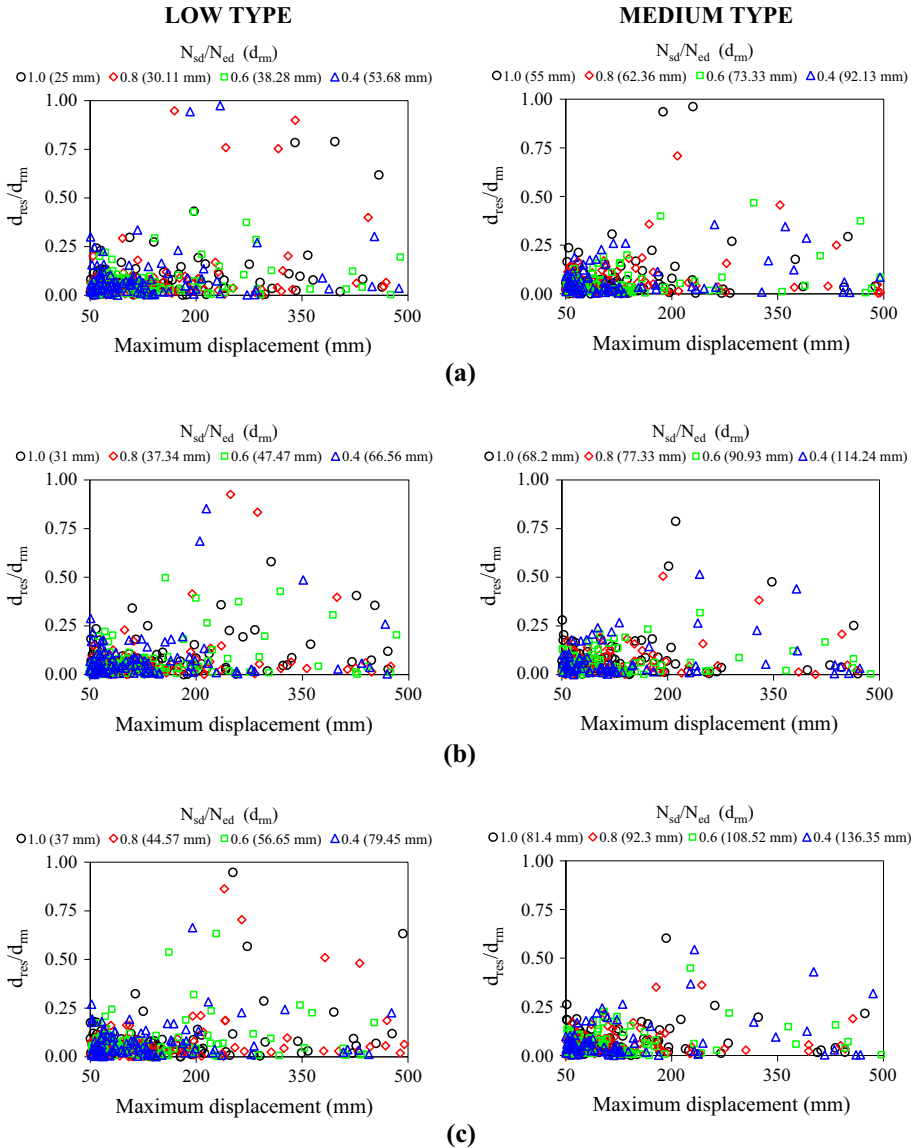


Fig. 8 Residual displacement ratio (d_{res}/d_{rm}) vs. maximum displacement (d_{max}) obtained from nonlinear response history analysis of FPS with **a** $R = 2,500$ mm, **b** $R = 3,100$ mm and **c** $R = 3,700$ mm

the selected seismic ground motions range from approximately 1 mm to some 100 mm. As expected, the actual ground residual displacement d_{res} tends to increase while increasing the maximum (static) residual displacement d_{rm} of the isolation system, i.e. as the radius of curvature increases (see Fig. 7c) and/or the axial load ratio reduces (see Fig. 7b).

Figure 8 shows the analysis results disaggregated by radius of curvature and axial load ratio. For more clarity, results have been normalized dividing the actual residual displacements by the corresponding maximum (static) residual displacement, to check the satisfaction of

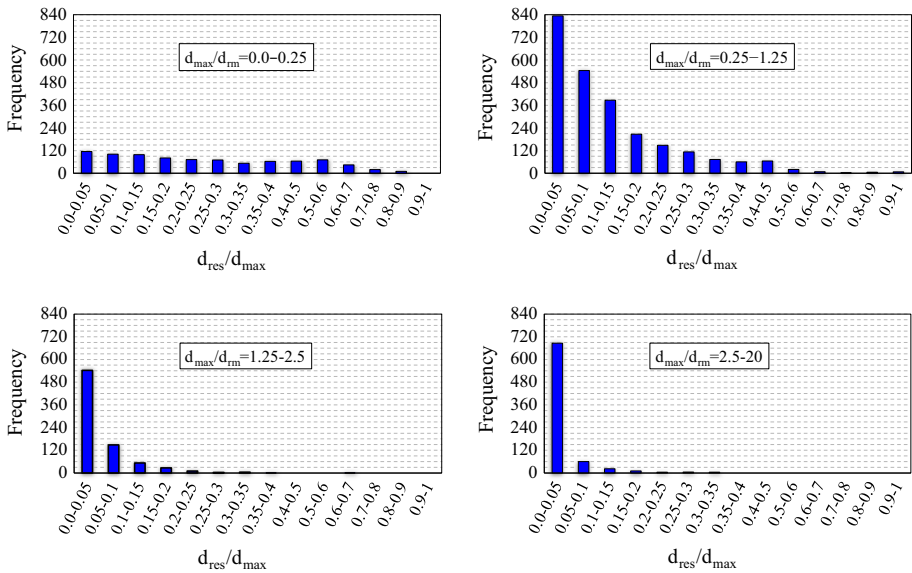


Fig. 9 Scattering of normalized residual displacements d_{res}/d_{max} in different ranges of the ratio d_{max}/d_{rm}

the inequality $d_{res} \leq d_{rm}$. It is interesting to note that the aforesaid condition is always satisfied although there are some cases (approximately a dozen) in which the actual residual displacement registered at the end of a single ground motion is very close to the maximum (static) residual displacement of the isolation system.

In Fig. 9 the distribution of the actual residual displacements d_{res} normalized with respect to the corresponding maximum seismic displacement d_{max} is presented in the form of histograms as a function of the ratio d_{max}/d_{rm} . The recorded data are grouped into data bins defined by intervals of d_{res}/d_{max} with width equal to 0.05. Four different ranges of the ratio d_{max}/d_{rm} are considered, namely: $0 < d_{max}/d_{rm} \leq 0.25$; $0.25 < d_{max}/d_{rm} \leq 1.25$; $1.25 < d_{max}/d_{rm} \leq 2.5$ and $2.5 < d_{max}/d_{rm} \leq 20$. It should be observed that when d_{max}/d_{rm} tends to zero (i.e. FPS with low restoring force) the distribution of normalized residual displacements d_{res}/d_{max} is almost uniform. The shape of the distribution changes significantly as the ratio d_{max}/d_{rm} increases and the most probable values of d_{res}/d_{max} result lower than 5%. This seems to suggest that, all other things being equal, the re-centring capability of the isolation system tends to improve when the maximum displacement of the isolation system is sufficiently higher than the maximum (static) residual displacement. However, it should be noted that d_{max} and d_{rm} are intrinsically correlated. Indeed, both depend on μ and R . Thus, it makes no sense to express the re-centring capability of FPS in terms of d_{max} independently from d_{rm} .

For all the cases herein considered, there is a significant dispersion in the observed data, which reflects the strong dependence of the seismic response (and in particular of the residual displacement) on the characteristics of the seismic ground motion, as well as the wide variability of the system parameters used in the analysis.

In Fig. 10 the normalized residual displacements d_{res}/d_{max} are presented as a function of the ratio d_{max}/d_{rm} , separately for low-type and medium-type friction FPSs. It's worth noting that the maximum value of the ratio d_{res}/d_{max} registered in this study results equal to approximately 0.9 while the maximum value of the ratio d_{max}/d_{rm} is equal to approximately 19. As can be seen, the ratio d_{res}/d_{max} tends to decrease as the ratio d_{max}/d_{rm} increases. In

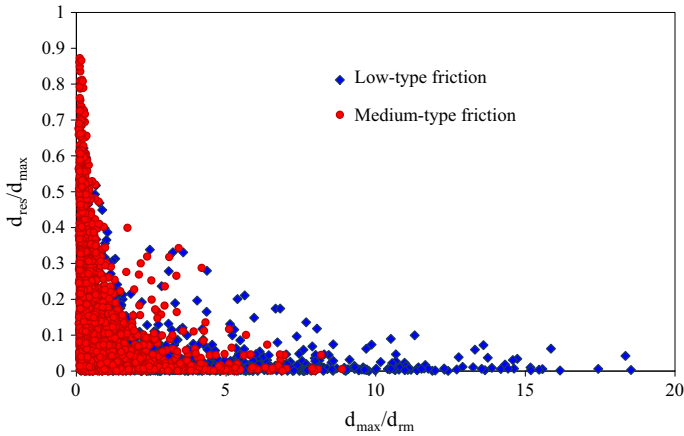


Fig. 10 Values of normalized residual displacements d_{res}/d_{max} obtained from NRHA as a function of the ratio d_{max}/d_{rm} for low- and medium-type friction FPSs

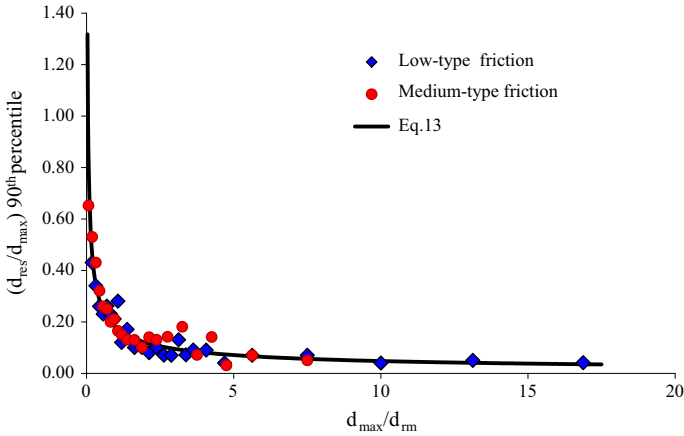


Fig. 11 Regression analysis (90th percentile) of the observed values of the normalized residual displacement d_{res}/d_{max} as a function of the ratio d_{max}/d_{rm} for low- and medium-type friction FPSs

other words, from a statistical point of view, the residual displacement tends to be negligible compared to the maximum seismic displacement when the ratio d_{max}/d_{rm} turns out to be relatively large and vice-versa.

Due to the large scatter in the observed data, the 90th percentile (i.e. 90% of the observed values do not exceed this value) is proposed as a possible reference value for design considerations. In Fig. 11, the 90th percentile of the normalized residual displacements d_{res}/d_{max} is reported as a function of the normalized maximum displacement d_{max}/d_{rm} . It should be noted that the 90th percentile of the observed data has been evaluated considering intervals of d_{max}/d_{rm} of increasing width, e.g. for low-type friction FPSs: 0.05 for $0.0 < d_{max}/d_{rm} < 1.25$; 0.1 for $1.25 < d_{max}/d_{rm} < 3.75$; 0.25 for $3.75 < d_{max}/d_{rm} < 5.0$; 0.5 for $5.0 < d_{max}/d_{rm} < 6.25$; 1.0 for $6.25 < d_{max}/d_{rm} < 11.25$ and 1.5 for $11.25 < d_{max}/d_{rm} < 18.75$. The 90th percentile regression curve indicate that there is a strong correlation with the ratio d_{max}/d_{rm} while the dependence on the friction

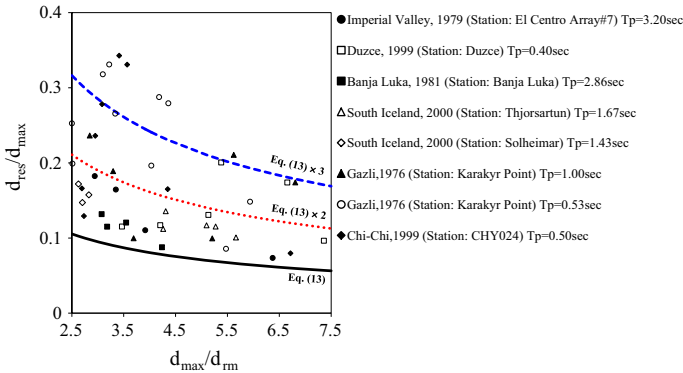


Fig. 12 Outliers due to pulse-like effects and proposed correction factors

coefficient is quite negligible (differences less than 10% in terms of multiplying factor in Eq. (13), considering separately low- and medium-type FPSs), probably because the effect of the friction coefficient is already included in the maximum residual displacement d_{rm} (see Eq. 6).

As can be seen, when the ratio d_{max}/d_{rm} is greater than 2.5, the 90th percentile of the normalized residual displacement d_{res}/d_{max} turns out to be practically independent from d_{max}/d_{rm} . In other words, the value of the residual displacement d_{res} tends to be the same for all the earthquakes that induce maximum displacement $d_{max} > 2.5d_{rm}$, with values of d_{res} relatively small compared to d_{max} (i.e. $d_{res}/d_{max} < 0.10$). Based on this observation, as a general rule of thumb, a suitable re-centring capability can be expected for FPS when the ratio d_{max}/d_{rm} is > 2.5 , regardless the characteristics of the earthquake and individual values of R and μ .

It is worth noting that, in the range $2.5 \leq d_{max}/d_{rm} \leq 7.5$ (see Fig. 10), a number of individual points characterized by values of the ratio d_{res}/d_{max} significantly greater than those predicted by the regression curve of Fig. 11 is observed. For sake of clarity, Fig. 12 shows the points in the range $2.5 \leq d_{max}/d_{rm} \leq 7.5$ featuring values of d_{res}/d_{max} greater than the 1.1 times those predicted by the proposed relationship (see Eq. 13). Actually, all these points correspond to near-fault earthquakes classified as pulse-like by (Baker 2007) and characterized by values of the pulse period T_p ranging from 0.50 to 3.50 s. It is then apparent that, at least in the range of values of d_{max}/d_{rm} under consideration, the proposed relationship may underestimate the actual residual displacements of FPS in case of pulse-like near-fault earthquakes. In these cases, an amplification factor should be applied to estimate with some accuracy the residual displacement of FPS. Based on the results of this study, in first approximation, an amplification factor of the order of 2.0, for pulse-like near-fault earthquakes with $1.5 \leq T_p \leq 3.5$ (see Fig. 12), and around 3.0, for pulse-like near-fault earthquakes with $0.5 \leq T_p \leq 1.0$ (see Fig. 12), may be adopted for a rough estimate of the expected residual displacement. Further studies are needed to fully understand the dependency of residual displacements on the characteristics of pulse-like earthquakes.

4.3 Design tool for the estimation of the residual displacement of FPS

The main product of this study is represented by the regression curve of Fig. 11, which provides the expected residual displacement (90th percentile of the observed data) as a func-

tion of the maximum transient displacement d_{max} and maximum static residual displacement $d_{rm} (= \mu_{slow}R)$. Based on the nonlinear regression analysis performed, the expected residual displacement of FPS can be estimated with the following equation ($R^2 = 0.91$):

$$d_{res(90th)} = 0.18 d_{max} \left(\frac{d_{max}}{d_{rm}} \right)^{-0.57} \quad (13)$$

which can be approximated by the simpler expression:

$$d_{res(90th)} = 0.18 \sqrt{d_{max} d_{rm}} \quad (14)$$

Equation (14) coincides with Eq. (13) for $d_{max}/d_{rm} = 2.5$. For $0.25 < d_{max}/d_{rm} < 2.5$ ($2.5 < d_{max}/d_{rm} < 10$), Eq. (14) underestimates (overestimates) Eq. (13), with errors less than 10%. For $10 < d_{max}/d_{rm} < 20$, Eq. (14) overestimates Eq. (13), with errors that never exceed 15%.

According to Eq. (13), Fig. 13a shows the variability of d_{res} for six different values of d_{rm} , ranging from 25 to 150 mm, which are compatible with the characteristics (μ and R) of currently used standard FPSs. As expected, for a given value of the ratio d_{max}/d_{rm} , the re-centring capability of FPS reduces as the value of d_{rm} increases (e.g. when the friction coefficient, for a given radius of curvature, increases). Based on Fig. 13a, the 90th percentile of the residual displacement, for the low-type friction FPSs considered in this study, increases from approximately 5 mm (for $d_{max}/d_{rm} = 2.5$ and $d_{rm} = 25$ mm) to approximately 45 mm (for $d_{max}/d_{rm} = 18.75$ and $d_{rm} = 75$ mm). For d_{max}/d_{rm} lower than 2.5, the expected residual displacement d_{res} does not exceed 20 mm. Similarly, the residual displacement of medium-type friction FPS increases from approximately 15 mm (for $d_{max}/d_{rm} = 2.5$ and $d_{rm} = 50$ mm) to approximately 95 mm (for $d_{max}/d_{rm} = 18.75$ and $d_{rm} = 150$ mm). For d_{max}/d_{rm} lower than 2.5, the expected residual displacement d_{res} does not exceed 35 mm.

The diagram of Fig. 13a can be seen as a useful tool for the estimation of the residual displacement of FPS (with 10% of probability of being exceeded), based on the maximum (static) residual displacement d_{rm} and the expected maximum transient displacement d_{max} . The former, indeed, depends only on the main mechanical parameters of FPS (R and μ_{slow}) while the latter can be obtained from linear structural analysis (e.g. linear dynamic analysis with response spectrum) for different limit states of the structure. Obviously, for a given value of d_{rm} , larger values of both maximum and residual displacement are expected for higher PGA values, corresponding to limit states with longer periods of return. Statistically speaking, Fig. 13a points out that d_{max} increases more rapidly than d_{res} while increasing the seismic intensity of the expected ground motion.

According to current seismic codes (AASHTO 2000; CBSC 2001; IBC 2006; CEN 2005), isolation devices and their connections to the structure must be designed and constructed in such a way that their performance characteristics conform with given design requirements at both Serviceability Limit State (SLS) and Collapse Prevention Limit State (CPLS). Isolation devices responding according to SLS, in particular, can undergo only very minor or superficial damage, which should not induce interruption of use, nor require any repair. Moreover, possible residual displacements at the end of the earthquake must be compatible with the serviceability of the structure as a whole, including non-structural components and utilities. On the other hand, isolation devices responding according to CPLS can suffer damage, but shall not reach failure. Replacement of the devices after any damage shall be possible with minor efforts. Moreover, they must retain a suitable residual displacement capacity towards further seismic events that may occur after the main shock.

It is clear that the fulfillment of the aforesaid design requirements is directly or indirectly related to the acceptability of the residual displacements of the isolation system. In particular,

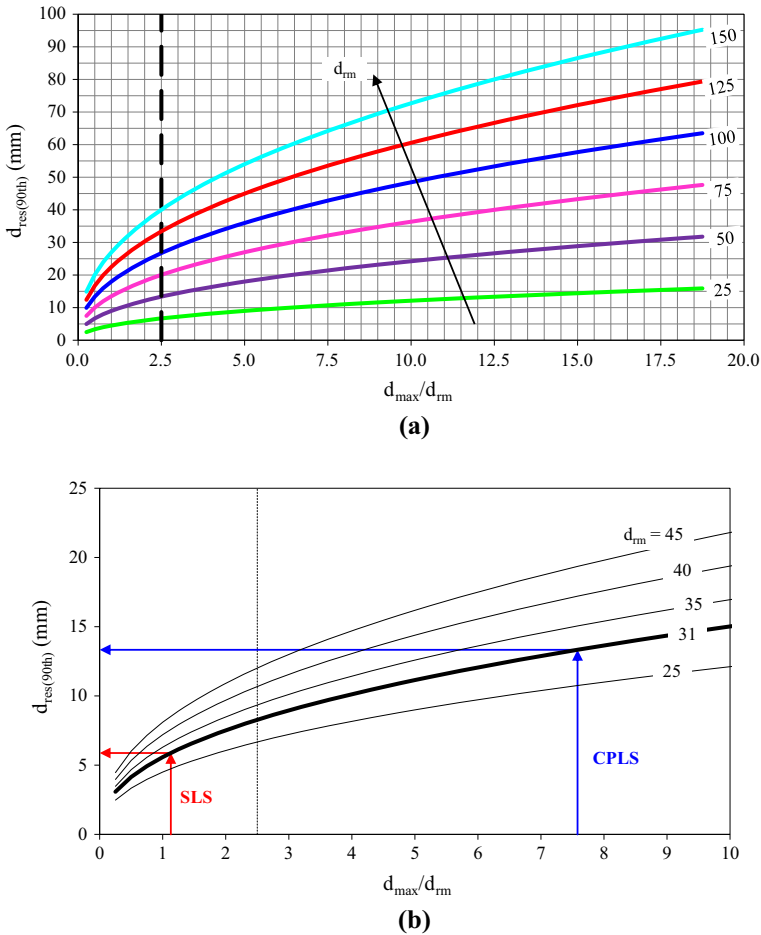


Fig. 13 **a** Design tool for the estimation of the expected (90th percentile) residual displacement, **b** example of application for FPS with $R = 3,100$ mm, $\mu_{fast} = 2.5\%$ and $\mu_{slow} = 1\%$. *SLS* Serviceability Limit State, *CPLS* Collapse Prevention Limit State

the importance of checking the acceptability of the expected residual displacements at the SLS is self-apparent. The proposed criterion, however, can be useful also for the CPLS, when the design displacement is very close to the maximum displacement capacity of the isolation system. In that case, indeed, a not negligible residual displacement (e.g. greater than 10 % the maximum seismic displacement) may jeopardize the displacement capacity of the isolation system considering possible aftershocks and future earthquakes. It should be noted that FPSs typically feature an extra stroke (often not declared by the manufacturer) of the order of 10 % the nominal displacement capacity. Thus, even if the design displacement is almost equal to the displacement capacity, a residual displacement less than 10 % the maximum displacement can be accepted, relying on the aforesaid extra stroke.

As an example, the above said approach is applied to a FPS featuring $R = 3,100$ mm, $\mu_{fast} = 2.5\%$, $\mu_{slow} = 1.0\%$ ($d_{fm} = 31.0$ mm) and $d_m = 250$ mm, considering elastic response spectra compatible with the seismic hazard of the city of L’Aquila (Italy), for soil type B,

according to the Italian seismic code (NTC 2008) (see Fig. 13b). The maximum transient displacements, derived from spectral analysis, considering an equivalent visco-elastic model for FPS, are equal to approximately 35 mm at SLS and 235 mm at CPLS, respectively. As a consequence, the corresponding values of d_{\max}/d_{rm} are equal to approximately 1.13 and 7.58, respectively. According to the Eq. (13), the expected residual displacement of the isolation system increases from approximately 5.9–13.3 mm, passing from SLS to CPLS. At a glance, the CPLS residual displacement appears to be acceptable, being less than 10% the corresponding maximum displacement (235 mm). More precisely, it can be stated that, according to the proposed approach, the estimated residual displacement (13.3 mm) has 90% of probability of not be exceeded; in the remaining cases (10% probability of occurrence) the residual displacement will never exceed 31.0 mm. In other words, the maximum displacement in case of aftershocks or future earthquakes has 90% probability of not exceeding $13.3 + 235 = 248.3 \text{ mm} < 250 \text{ mm}$; in the remaining cases (10% probability of occurrence), it will never exceed $31 + 235 = 266 \text{ mm} < 1.1 \times 250 = 275 \text{ mm}$, even considering the possibility of accumulation of residual displacements after a sequence of seismic ground motions. At SLS, the rule of thumb $d_{\max}/d_{\text{rm}} > 2.5$ may result too conservative, due to the small values of maximum displacement involved. In that case, the SLS residual displacement shall be estimated using Eq. (13); details and specifications of non-structural components and utilities shall be then checked, to decide whether the SLS residual displacement is acceptable or not.

Generally speaking, the designer should always express his judgment about the acceptability of the expected residual displacement (at both limit states), also considering possible imprecisions during device installation, concerns related to the maintenance plan of the devices and, last but not least, the possibility of near-fault pulse-like earthquakes.

4.4 Accrual of residual displacement due to sequences of earthquakes

Accumulation of residual displacement may be a concern for FPS and it must be carefully examined within a realistic scenario.

Figure 14 shows the displacement-time histories of a medium-type friction FPS ($R = 3,100 \text{ mm}$, $\mu_{\text{fast}} = 9.2\%$, $\mu_{\text{slow}} = 3.6\%$) recorded during two real sequences of seismic ground motions characterized by one main-shock and one or two aftershocks registered, on the same day, by the same station. The details of the two sequences of earthquakes are reported in Table 3.

As can be seen, residual displacements tend to accumulate to a larger value in the first sequence of seismic ground motions. On the contrary, permanent displacements reverse and end up being almost zero at the end of the second sequence of seismic ground motions. The values of maximum and residual displacements registered during and at the end of each seismic ground motion are reported in Table 3.

Recently, Sarlis et al. (2013) performed shaking table tests of a 3-story seismically isolated structure equipped with triple friction pendulum isolators. In particular, they tested three configurations of FPS, considering two simulated sequences of low-to-moderate and high amplitude seismic ground motions, respectively. In this study, the sequence A of low-to-moderate amplitude ground motions, used in (Sarlis et al. 2013) for shaking table tests, is adopted for additional numerical analyses. Details on the selected (14) ground motions are reported in Table 3 (ref. to Sequence 3). In accordance with Sarlis et al. (2013), the original accelerations of each ground motion have been multiplied by a given scale factor (A in Table 3). Similarly, the duration of each ground motion has been multiplied by a given time scale factor (t in Table 3). Figure 15 shows the displacement response of two medium-type friction

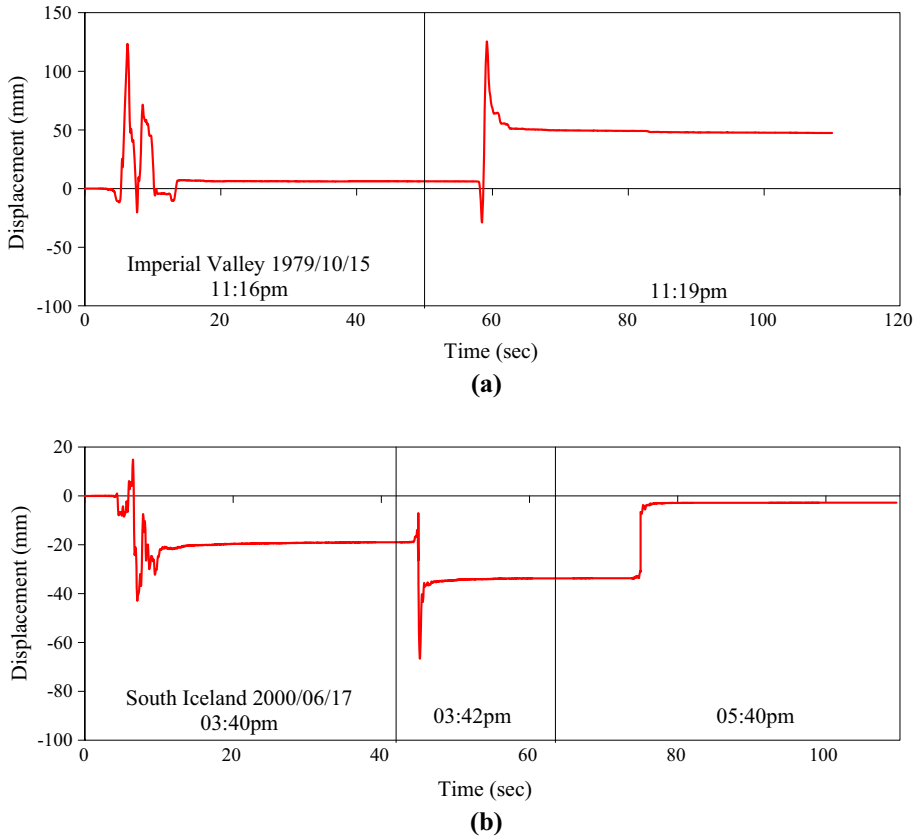


Fig. 14 Accrual of residual displacements due to real sequences of seismic ground motions: **a** Imperial Valley (1979/10/15) and **b** South Iceland (2000/06/17)

FPSs (with axial load ratio of 0.4 and radius of curvature equal to 2,500 and 3,700 mm, respectively), due to the simulated sequence of ground motions under consideration. As can be seen, the residual displacement results almost negligible during the first part of the sequence, then, it rapidly increases, attaining a cumulative value very close to the maximum residual displacement d_{rm} of each system, finally, it gradually reduces to lower values in the last part of the sequence.

In summary, the analysis results presented in this section show that the residual displacements may accumulate to a larger value after a sequence of earthquakes. A subtraction of residual displacements, however, can be just as probable as a summation. Thus, a structure experiencing a large residual displacement during an earthquake may eventually re-center when another earthquake occurs. All depends on the sequence of earthquakes and their characteristics.

To conclude, accumulation of residual displacements may be a concern for FPS, but never forgetting that the total residual displacement can never exceed d_{rm} . Further analyses, considering a lot of real sequences of seismic records, are needed for a better understanding of this phenomenon.

Table 3 Sequences of seismic ground motions considered in the analysis

Sequence	Seismic event(s)	Station	PGA (g)	A*	t**	FPS					
						R = 2,500 mm		R = 3,100 mm		R = 3,700 mm	
						d _{max}	d _{res}	d _{max}	d _{res}	d _{max}	d _{res}
1	Imperial Valley 1979/10/15	El Centro Array#5	0.55	1.00	1.00	–	–	127	6	–	–
			0.23	1.00	1.00	–	–	124	47	–	–
2	South Iceland 2000/06/17	502 Thjorsarbru	0.52	1.00	1.00	–	–	–43	–19	–	–
			0.26	1.00	1.00	–	–	–65	–35	–	–
			0.29	1.00	1.00	–	–	–33	–3	–	–
3	Northridge 1994/01/17	CDMG 24514 Sylmar-Olive View Med FF	0.84	1.00	0.50	95	–5	–	–	110	–11
				0.50	0.65	54	–3	–	–	57	–13
				0.50	0.50	–38	0	–	–	–56	–21
				1.00	0.70	–91	–5	–	–	–115	–14
	San.Fernando 1971/02/09	CDMG 279 Pacoima Dam	1.22	0.50	0.50	–136	–12	–	–	–150	–8
				0.80	0.50	–93	–88	–	–	–98	–92
				1.00	0.50	–103	–82	–	–	–121	–109
	Kobe 1995/01/16	0 KJMA	0.82	1.50	0.50	–99	–78	–	–	–133	–121
				0.50	0.50	–84	–77	–	–	–138	–135
				1.00	0.50	–112	–87	–	–	–151	–117
	Northridge 1994/01/17	USGS.0637 Sepulveda VA	0.75	1.50	0.50	–120	–76	–	–	–142	–102
				0.50	0.50	–85	–61	–	–	–111	–76
			1.00	0.50	–86	–50	–	–	–103	–52	
Chi-Chi, Taiwan 1999/09/20	CHY024	0.28	1.00	1.0	–148	–24	–	–	–172	–67	

* A multiplies accelerations of original ground motion

** t multiplies time step of the ground motion

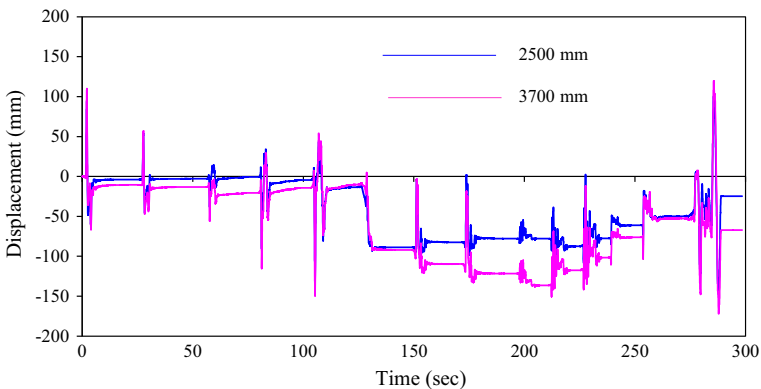


Fig. 15 Accrual of residual displacements due to simulated sequences of seismic ground motions (see Sequence 3 in Table 3)

5 Evaluation of current code requirements

Based on the results of this study, the main parameter that affects the restoring capability of FPS is the ratio d_{max}/d_{rm} . It has been concluded that, from a statistical perspective, FPSs with d_{max}/d_{rm} greater than 2.5 exhibit good restoring capability ($d_{res}/d_{max} < 0.1$), regardless the characteristics of FPS (R and μ) and seismic ground motion (see Fig. 10). Assuming, in first approximation, the maximum seismic displacement d_{max} equal to the design displacement d_d of the isolation system, the ratio d_{max}/d_{rm} can be re-written as $d_d/(\mu_{slow}R)$. As a consequence, the re-centring criterion proposed in this study for FPSs can be expressed as follows:

$$d_d/R \geq 2.5 \mu_{slow} \quad (15)$$

This allows for a direct comparison of the compliance criterion proposed in this study, for the re-centring capability of FPS, with current code requirements.

Both the 2000 AASHTO Guidelines (AASHTO 2000) and the 2001 California Building Code (CBSC 2001) essentially compare the increment of the post-elastic force to a certain fraction of the weight of the structure. They do not take specifically into account the magnitude of the characteristic strength F_0 (equal to μW for FPS), which is the main reason for insufficient re-centring capability of the isolation system. For FPS, $K_p = W/R$ and Eqs. (1)–(2) can be re-written as follows:

$$d_d/R \geq \beta \quad (16)$$

where β is equal 0.025 for 2000 AASHTO Guidelines and 0.05 for 2001 CBSC provisions, respectively.

Comparing Eq. (16) with Eq. (15), the following observations can be done: (i) for sliding isolation systems with $\mu_{slow} = 0.01$ (AASHTO) or $\mu_{slow} = 0.02$ (CBSC), the two expressions are identical; (ii) for sliding isolation systems with $\mu_{slow} > 0.01$ (AASHTO) or $\mu_{slow} > 0.02$ (CBSC), the requirements of the US Codes are less conservative than the compliance criterion proposed in this study. It is worth noting that the International Code Council (IBC 2006) allows isolation systems that do not comply with restoring capability criteria to be used if they remain stable under the full load and up to 3 times the design displacement (e.g. due to accumulation of residual displacement due to aftershocks or sequences of seismic ground motions). Based on the results of this study, this requirement appears too conservative for FPS, for which the expected residual displacements never exceed d_{rm} , which, in turn, results lower than 50% d_m (see Table 2).

The importance of the characteristic strength F_0 in determining the re-centring capability of the isolation system is recognized in the Eurocode 8—Part 2 provisions (CEN 2005), through the definition of the so-called maximum residual displacement d_{rm} (see Eq. 4). It is worth noting that, according to the EC8 provisions, the maximum displacement capacity d_m , used in Eq. (4), is defined as the maximum displacement that the isolator can sustain, which includes the design displacement obtained from seismic analysis (d_d) plus other displacement components such as those due to the long-term effects and thermal loadings. Assuming, in first approximation, the maximum displacement capacity d_m equal to the design displacement d_d of the isolation system, expression (4) can be simplified as follows:

$$K_p d_d \geq \sqrt{0.03\mu} W \quad (17)$$

where μ is the ratio of the characteristic strength to weight, equal to the coefficient of friction at slow velocity for sliding isolation systems. For FPSs, Eq. (17) can be re-written as follows:

$$d_d/R \geq \sqrt{0.03\mu} \quad (18)$$

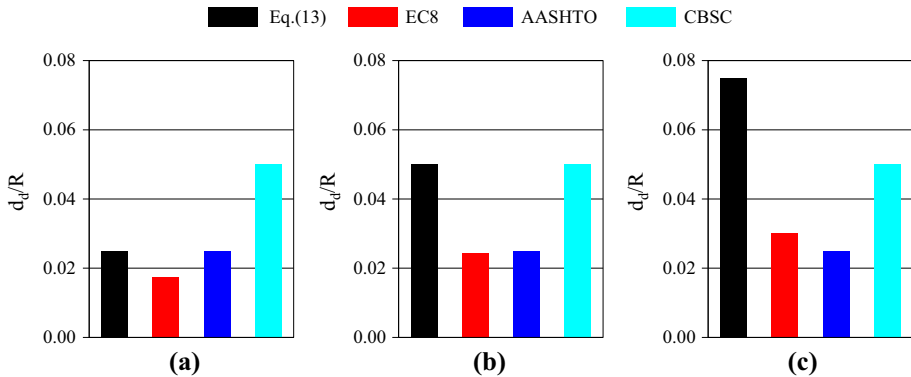


Fig. 16 Comparisons between the proposed re-centring compliance criterion ($d_{max}/d_{rm} > 2.5$) and the restoring capability provisions adopted in current seismic codes, for three different values of dynamic-slow friction coefficient (μ_{slow}), namely: **a** 1 %, **b** 2 % and **c** 3 %

Equation (18) coincides with the compliance criterion proposed in this study for $\mu_{slow} \approx 0.5\%$, while for $\mu_{slow} > 0.5\%$ the EC8 requirement turns out to be less conservative than that proposed in this study. Figure 16 compares the four restoring requirements under examination, for three typical values of the friction coefficient at slow velocity (namely 1, 2 and 3 %).

Finally, it should be observed that all the low-type friction FPSs of Table 2 comply with the restoring capability requirement proposed in this study (see Eq. 15) when the CPLS design displacement is relatively close to the maximum displacement capacity of the device (say $d_d > 0.8d_m$) and the quasi-permanent vertical load is sufficiently close to the maximum load capacity of the device (say $N_{sd} > 0.7N_{Ed}$). For the medium-type friction FPSs, more restrictive conditions apply and the proposed re-centring compliance criterion may not be satisfied for the devices with lower maximum displacement capacity. As said before, however, it is always recommended to evaluate the expected residual displacements (using Eq. 13) and judge whether they are acceptable or not, considering all possible issues that could adversely affect the expected residual displacements, such as possible imprecisions during device installation, low-temperature effects (Dolce et al. 2005), maintenance concerns, possibility of pulse-like earthquakes, etc.

6 Conclusions

In this paper, the results of extensive parametric analyses on the restoring capability of Friction Pendulum seismic isolation Systems (FPSs) have been presented. Residual displacements have been obtained from Non-linear response history analyses of SDOF systems considering commercial values of the radius of curvature (R) and typical values of dynamic-fast (μ_{fast}) and dynamic-slow (μ_{slow}) friction coefficient, ranging approximately from 2.5 to 9.2 % and from 1.0 to 3.7 %, respectively, based on the level of bearing pressure. A set of 230 real seismic ground motions has been used to evaluate, from a statistical perspective, the restoring capability of FPSs. Based on the results of this study the following conclusions can be drawn:

1. The main parameter that affects the restoring capability of FPS is the ratio d_{max}/d_{rm} , where d_{max} is the maximum seismic displacement and d_{rm} is the maximum (static)

residual displacement, equal to $\mu_{\text{slow}} R$ for FPS, where μ_{slow} is the dynamic(-slow) friction coefficient and R the radius of curvature of the device;

2. As d_{max} includes the effects of seismic excitation, the restoring capability of FPS depends not only on the isolation system properties (through d_{rm}) but also on the earthquake characteristics, resulting generally better (lower $d_{\text{res}}/d_{\text{max}}$ ratios) for earthquakes causing greater maximum displacements;
3. FPSs with $d_{\text{max}}/d_{\text{rm}} > 2.5$ experience negligible residual displacements compared to their corresponding maximum transient displacements ($d_{\text{res}} < 0.1d_{\text{max}}$);
4. A simple relationship (see Eq. 13) has been proposed to predict the residual displacement of FPSs. In presence of near-fault pulse-like earthquakes, amplification factors as high as 2–3 should be applied to Eq. (13) to estimate residual displacements with some accuracy;
5. Residual displacements may accumulate during a sequence of earthquakes, including a mainshock and one or more aftershocks. A subtraction of residual displacements, however, can be just as probable as a summation. The accrual of residual displacement, therefore, may be a concern for FPS, but never forgetting that the total residual displacement can never exceed d_{rm} .
6. Comparisons between the proposed re-centring compliance criterion ($d_{\text{max}}/d_{\text{rm}} > 2.5$) and the restoring capability provisions adopted in current seismic codes (AASHTO 2000; CBSC 2001; CEN 2005; IBC 2006) show that these latter are generally little conservative for currently used FPSs. Further considerations on possible imprecisions during the installation of the devices, low-temperature effects and issues related to the maintenance of the devices during the life-cycle of the structure call for a more prudential estimate of the residual displacements of FPSs, as proposed in this study.

Acknowledgments This work has been partially funded by the ReLUIIS (Laboratories University Network of Seismic Engineering) Consortium within the ReLUIIS/DPC 2014–2018 research program (Research line: Seismic Isolation & Energy Dissipation).

References

- AASHTO (2000) Guide Specifications for Seismic Isolation Design-Interim 2000. American Association of State Highways and Transportation Officials, Washington, DC
- Alavi B, Krawinkler H (2001) Effects of near-fault ground motions on frame structures, Blume Center Report 138, Stanford, California
- Al-Hussaini TM, Zayas VA, Constantinou MC (1994) Seismic isolation of a multi-story frame structure using spherical sliding isolation systems, Technical Report No. NCEER-94-0007, National Center for Earthquake Engineering Research, Buffalo, NY
- Anderson JC, Bertero VV (1987) Uncertainties in establishing design earthquakes. *J Struct Eng* 113(8):1709–1724
- ASCE/SEI 7 (revision for 2016) Minimum design loads for buildings and other structures, American Society of Civil Engineers, 1801 Alexander Bell Drive Reston, VA 20191
- Baker JW (2007) Quantitative classification of near-fault ground motions using wavelet analysis. *Bull Seismol Soc Am* 97(5):1486–1501
- Bertero V, Mahin S, Herrera R (1978) Aseismic design implications of near-fault San Fernando earthquake records. *Earthq Eng Struct Dyn* 6(1):31–42
- Berton S, Infanti S, Castellano MG, Hikosaka H (2006) Self-centring capacity of seismic isolation systems. *Struct Control Health Monit* 14(6):895–914
- Braun C, Medeot R (2000) New design approaches to reduce seismic risk—mitigation of seismic risk support to recently affected European Countries. Belgirate, Italy
- Cardone D, Dolce M, Gesualdi G (2009) Lateral force distributions for the linear static analysis of base-isolated buildings. *Bull Earthq Eng* 7:801–834
- Cardone D, Dolce M, Palermo G (2010) Direct displacement-based design of buildings with different seismic isolation systems. *J Earthq Eng* 14(2):163–191

- Cardone D (2012) Re-centring capability of flag-shaped seismic isolation systems. *Bull Earthq Eng* 10:1267–1284
- CBC (2001) California building code. California Buildings Standards Commission, Sacramento
- CEN (2005) Eurocode 8: design of structures for earthquake resistance—Part 2: Bridges, EN1998-2:2005. European Committee for Standardization, Bruxelles, Belgium
- Constantinou MC, Caccese J, Harris HG (1987) Friction characteristics of PTFE-steel interfaces under dynamic conditions. *Earthq Eng Struct Dynam* 15(6):751–759
- Constantinou M, Mokha A, Reinhorn AM (1990) Teflon bearings in base isolation. II: modeling. *J Struct Eng* 116(2):455–474
- Constantinou MC, Whittaker AS, Kalpakidis Y, Fenz DM, Warn GP (2007) Performance of seismic isolation hardware under service and seismic loading. Technical Report MCEER-07-0012, Multidisciplinary Center for Earthquake Engineering Research, State University of New York at Buffalo, Buffalo, NY
- Dicleli M, Buddaram S (2006) Effect of isolator and ground motion characteristics on the performance of seismic-isolated bridges. *Earthq Eng Struct Dyn* 35(2):223–250
- Dolce M, Cardone D, Croatto F (2005) Frictional behaviour of steel-PTFE interfaces for seismic isolation. *Bull Earthq Eng* 3(1):75–99
- FIP Industriale (2013) Catalogue S04—Curved Surface Sliders, Padova, Italy. Available on-line at <http://www.fipindustriale.it>
- Hwang JS, Chang KC, Lee GC (1990) Quasi-static and dynamic characteristics of PTFE-stainless interfaces. *J Struct Eng* 116(10):2747–2762
- IBC (2006) International Building Code. International Code Council, Falls Church
- Ismail M, Rodellar J, Pozo F (2014) An isolation device for near-fault ground motions. *Struct Control Health Monit* 21:249–268
- Katsaras CP, Panagiotakos TB, Koliias B (2008) Restoring capability of bilinear hysteretic seismic isolation systems. *Earthq Eng Struct Dyn* 37:557–575
- Kawashima K, MacRae GA, Hoshikuma J, Kazuhiro N (1998) Residual displacement response spectrum. *J Struct Eng (ASCE)* 124(5):523–530
- Kelly TE (2001) Base isolation of structures: design guidelines. Holmes Consulting Group Ltd, New Zealand
- Luco N, Cornell CA (2007) Structure-specific scalar intensity measures for near-source and ordinary earthquake ground motions. *Earthq Spectra* 23(2):357–392
- MacRae GA, Kawashima K (1997) Post-earthquake residual displacements of bilinear oscillators. *Earthq Eng Struct Dyn* 26(7):701–716
- Mahin SA, Bertero VV (1981) An evaluation of inelastic seismic response spectra. *J Struct Div (ASCE)* 107(9):1777–1795
- Mavroedidis GP, Dong G, Papageorgiou AS (2004) Near-fault ground motions, and the response of elastic and inelastic single degree-of-freedom (SDOF) systems. *Earthq Eng Struct Dyn* 33(9):1023–1049
- Medeot R (2004) Re-centring capability evaluation of seismic isolation systems based on energy concepts. In: Proceedings of the 13th world conference on earthquake engineering, Vancouver, Canada, Paper 3106
- Mokha A, Constantinou M, Reinhorn AM (1990) PTFE bearings in base isolation: testing. *J Earthq Eng* 116(2):438–454
- Mokha AS, Constantinou MC, Reinhorn AM (1991) Experimental study of friction-pendulum isolation system (ASCE). *J Struct Eng* 117:1201–1217
- Mokha A, Constantinou M, Reinhorn AM (1993) Verification of friction model of PTFE bearings under triaxial load. *J Struct Div (ASCE)* 119(1):240–261
- Naeim F, Kelly JM (1999) Design of seismic isolated structures. Wiley, New York
- Nagarajaiah S, Reinhorn AM, Constantinou MC (1991) 3D-Basis: non-linear dynamic analysis of three-dimensional base isolated structures: Part II, Technical Report NCEER-91-0005, National Center for Earthquake Engineering Research, State University of New York at Buffalo, Buffalo
- NTC (2008) Norme Tecniche per le Costruzioni, Decreto Ministeriale 14/01/2008, Rome (in Italian)
- Quaglini V, Dubini P, Poggi C (2012) Experimental assessment of sliding materials for seismic isolation systems. *Bull Earthq Eng* 10:717–740
- Riddell R, Newmark NM (1979) Statistical analysis of the response of nonlinear systems subjected to earthquakes, Research Report, University of Illinois, Urbana, IL
- SAP2000_Nonlinear (2014) Static and dynamic finite element analysis of structures. Berkeley, CA, USA
- Sarlis AA, Constantinou MC, Reinhorn AM (2013) Shake table testing of triple friction pendulum isolators under extreme conditions, Technical Report MCEER-13-0011, Multidisciplinary Center for Earthquake Engineering Research, State University of New York at Buffalo, Buffalo, NY
- Shin J, Kim JH, Lee K (2014) Seismic assessment of damaged piloti-type RC building subjected to successive earthquakes. *Earthq Eng Struct Dyn*. doi:10.1002/eqe.2412
- Skinner RI, Robinson WH, McVerry GH (1993) An introduction to seismic isolation. Wiley, New York

- Tsopelas P, Constantinou MC (1994) NCEER-TAISEI corporation research program on sliding seismic isolation systems for bridges-experimental and analytical study of a system consisting of sliding bearings and fluid restoring force/damping devices. Technical Report NCEER-94-0014, University of New York at Buffalo, Buffalo, NY
- Tsopelas P, Okamoto S, Constantinou MC, Ozaki D, Fujii S (1994) NCEER-TAISEI corporation research program on sliding seismic isolation systems for bridges-experimental and analytical study of systems consisting of sliding bearings, rubber restoring force devices and fluid dampers. Technical Report NCEER-94-0002, University of New York at Buffalo, Buffalo, NY